Manuscript prepared for Atmos. Meas. Tech.
with version 3.0 of the LaTeX class copernicus.cls.
Date: 9 December 2010

A geostationary thermal infrared sensor to monitor the lowermost troposphere: O_3 and CO retrieval studies

M. Claeyman[1,2], J.-L. Attié[1,2], V.-H. Peuch[2], L. El Amraoui[2], W. A. Lahoz[2,3], B. Josse[2], P. Ricaud[1], T. von Clarmann[4], M. Höpfner[4], J. Orphal[4], J.-M. Flaud[5], D. P. Edwards[6], K. Chance[7], X. Liu[7], F. Pasternak[8], and R. Cantié[8]

[1]Laboratoire d'Aérologie, Université de Toulouse, CNRS/INSU, Toulouse, France
[2]CNRM-GAME, Météo-France and CNRS URA 1357, Toulouse, France
[3]NILU, N-2027 Kjeller, Norway
[4]Karlsruhe Institute of Technology, IMK, Karlsruhe, Germany
[5]Laboratoire Interuniversitaire des Systèmes Atmosphériques, CNRS UMR 7583, Université de Paris-Est, Créteil, France
[6]National Center for Atmospheric Research, Boulder, Colorado, USA
[7]Harvard-Smithsonian Center for Astrophysics, Cambridge, MA 02138, USA
[8]Astrium-EADS, Toulouse, France

Correspondence to: M. Claeyman, Laboratoire d'aérologie 14 avenue Edouard Belin, 31400 Toulouse
(marine.claeyman@aero.obs-mip.fr)

Abstract. This paper describes the capabilities of a nadir thermal infrared (TIR) sensor proposed for deployment onboard a geostationary platform to monitor ozone (O_3) and carbon monoxide (CO) for air quality (AQ) purposes. To assess the capabilities of this sensor we perform idealized retrieval studies considering typical atmospheric profiles of O_3 and CO over Europe with different instrument configuration (signal to noise ratio (SNR) and spectral sampling interval (SSI)) using the KOPRA forward model and the KOPRA-fit retrieval scheme. We then select a configuration, referred to as GEO-TIR, optimized for providing information in the lowermost troposphere (LmT; 0-3 km in height). For the GEO-TIR configuration we obtain $\sim$ 1.5 degrees of freedom for O_3 and $\sim$ 2 for CO at altitudes between 0 and 15 km. The error budget of GEO-TIR, calculated using the principal contributions to the error (namely, temperature, measurement error, smoothing error) shows that information in the LmT can be achieved by GEO-TIR. We also retrieve analogous profiles from another geostationary infrared instrument with SNR and SSI similar to the Meteosat Third Generation Infrared Sounder (MTG-IRS) which is dedicated to numerical weather prediction, referred to as GEO-TIR2. We quantify the added value of GEO-TIR over GEO-TIR2 for a realistic atmosphere, simulated using the chemistry transport model MOCAGE (MOdèle de Chimie Atmospherique à Grande Echelle). Results show that GEO-TIR is able to capture well the spatial and temporal variability in the LmT for both O_3 and CO. These results also provide evidence of the significant added value in the LmT of GEO-TIR compared to GEO-TIR2 by showing GEO-TIR is closer to MOCAGE

than GEO-TIR2 for various statistical parameters (correlation, bias, standard deviation).

1 Introduction

Air quality (AQ) is associated with the near surface atmospheric composition of trace gases and particles (Seinfeld and Pandis, 1997; Menut and Bessagnet, 2010). AQ is quantified using standards of concentration and deposition levels based on scientific knowledge of the impact of these pollutants on human health and the environment. Among species targeted by European policies, some are of greater concern as they more frequently exceed regulatory thresholds and require the public to be informed if this happens, examples include ground-level ozone (O_3), nitrogen oxides (NO_x) and suspended particulate matter (PM). Emissions of atmospheric pollutants from human activities are monitored and regulated at the European level by directives focusing both on activity sectors and national ceilings. Monitoring estimated and declared emissions is a challenge, owing to the complexity and number of emission sources. Among these, combustion sources (traffic, industry, residential use) are major contributors and need to be better simulated by models (e.g., Cuvelier et al., 2007; Vautard et al., 2007). Carbon monoxide (CO), an O_3 precursor, is a good tracer for combustion processes, including wild fires (e.g., Turquety et al., 2009). O_3 is an irritant which can affect severely the respiratory tract, in particular for people suffering from respiratory diseases, children and the elderly.

In the troposphere, the variability of sinks (including chemical losses such as from deposition), source strengths and transport and mixing processes, induces significant short term variations (one hour or less) of reactive species concentration (e.g., NO_x). Relevant temporal (1 hour) and spatial sampling scales (10 km x 10 km) for observations are determined by: tropospheric lifetime of the species of interest; characteristic time scales for transport and mixing; horizontal scales characterizing heterogeneities of direct emission sources; and characteristic time scales of sinks (e.g., chemical sinks, deposition) and sources (e.g., photochemistry). Furthermore, for various AQ applications, it is also important to provide observations of unpredictable emissions like forest fires or industrial accidental releases. The challenge for space-borne observations relevant to AQ is to measure accurately tropospheric trace gas composition at adequate spatial and temporal resolution (Martin, 2008). Therefore, requirements to monitor AQ from space can be quantified, bearing in mind that they complement current information from *in-situ* measurements (e.g., from AQ networks, sondes, aircraft measurements). To complement this *in-situ* information, denser data sets with continental/global coverage in the lowermost troposphere (LmT; defined to be the atmosphere between 0 and 3 km) are needed for most species of interest (e.g., $O_3$and CO); these can only be provided by satellite observations.

Over the last few decades, space-borne observations of tropospheric composition (e.g., profiles and/or columns of O_3, CO) have been based on Low Earth Orbit (LEO) nadir viewing platforms:

ERS-2/GOME-1 (Global Ozone Monitoring Experiment, Burrows et al. (1999)); ADEOS/IMG (Interferometric Monitor for Greenhouse Gases, Kobayashi et al. (1999)); Terra/MOPITT (Measurement of Pollution in the Troposphere, Drummond and Mand (1996b)); Aqua/AIRS (Atmospheric InfraRed Sounder, McMillan et al. (2005)); Aura/TES (Tropospheric Emission Spectrometer, Beer et al. (2001)); Aura/OMI (Ozone Monitoring Instrument, Levelt et al. (2006)); METOP-A/IASI (Infrared Atmospheric Sounding Interferometer, Clerbaux et al. (2009)); METOP-A/GOME–2 Callies et al. (2000); ENVISAT/SCIAMACHY (Scanning Imaging Absorption Spectrometer for Atmospheric Chartography, Bovensmann et al. (1999)). Because LEO platforms sample representative regions once or twice a day, they are not well adapted to the temporal variability and spatial gradients generally exhibited by species of interest for AQ management and forecasts. From the point of view of AQ, the troposphere is thus significantly under-sampled. Continental-scale observations on atmospheric composition must be made at temporal resolutions appropriate for capturing the diurnal cycle (and shorter temporal time scales) in pollutants, and at spatial resolutions appropriate for capturing emissions and transcontinental transport of pollutants, or proxies for pollutants. The only observing platform that can provide this information is a geostationary (GEO) platform (Bovensmann and Orphal, 2005; Edwards, 2006). Typically a GEO covers one third of the Earth which is sufficient for covering Europe, our domain of interest concerning AQ. A GEO platform has the following desirable features: large scale observations that capture continental-scale emissions and processes (e.g., transport); repetitive observations to allow identification of temporal patterns and the production of long-term time-series; near simultaneous observations of key atmospheric composition variables; high temporal resolution observations to identify the temporal variability relevant to human society (e.g., diurnal and shorter time scales); and near-real-time observations for operational needs, as in Numerical Weather Prediction (NWP) and AQ forecasting.

Several GEO missions have been proposed for AQ. In the USA, the GEO-CAPE mission (Edwards et al., 2009; National Research Council, 2007) is being recommended for launch in the 2020-2022 timeframe. In Japan, a similar mission (Meteorology and Air Pollution-Asia (GMAP-Asia)) has been planned by the Japan Society of Atmospheric Chemistry to monitor O_3 and aerosols (including their precursors) from GEO (Akimoto et al. (2008); http://www.stelab.nagoya-u.ac.jp/ste-www1/div1/taikiken/eisei/eisei2.pdf, Japanese version only). In Korea, the Geostationary Environment Monitoring Spectrometer (Lee et al., 2010) is proposed to be launched in 2017-2018 onboard a GEO satellite, MP-GEOSAT of Korea Aerospace Research Institute. It would include an UV-Visible Spectrometer to monitor trans-boundary pollution events in Asia-Pacific region.

In Europe, the GeoTrope (Burrows et al., 2004) and GeoFIS (Flaud et al., 2004; Orphal et al., 2005) concept missions have been proposed to monitor tropospheric constituents at high temporal and spatial resolution. The Meteosat Third Generation - Thermal Infrared Sounder (MTG-IRS) is a planned mission to be launched from 2017. MTG-IRS will be able to provide information on horizontally, vertically, and temporally resolved water vapour and temperature structures of the

atmosphere. It will also provide O_3 and CO measurements in the troposphere within the long-wave infrared and the mid-wave infrared bands, respectively. The sentinel 4 UVN (ultraviolet-visible-near infrared) payload is also a planned mission and will be embarked on the two MTG - Sounder (MTG-S) satellites in GEO orbit over Europe; there are planned for launch from 2017 and 2024 and UVN is expected to provide measurements of O_3 and nitrogen dioxide columns, and aerosol optical depth. In order to complement the measurements provided by the Sentinel 4 UVN, the mission Monitoring the Atmosphere from Geostationary orbit for European Air Quality (MAGEAQ) has been proposed as a candidate for the Earth Explorer Opportunity Mission EE-8 call of the European Space Agency (Peuch et al., 2009, 2010). MAGEAQ is a multispectral instrument (thermal infrared and visible) designed to provide measurements of O_3 and CO in the LmT. Ozone is a key species for AQ purposes because of its impact on human health, ecosystem and climate (Seinfeld and Pandis, 1997); CO is a good tracer of pollution which allows the detection of unexpected pollution events such as wild fires (biomass burning) that impact AQ by long range transport (e.g., Pfister et al., 2004; Guerova et al., 2006).

Current AQ forecasting systems make little direct use of satellite measurements of chemical species, except through the use of global time-dependent chemical boundary conditions from global assimilation and forecast systems like the one demonstrated in the GEMS/MACC project (Global and regional Earth-system Monitoring using Satellite and in-situ data / Monitoring Atmospheric Composition and Climate), (Hollingsworth et al., 2008), or in the context of assessing biases and trends in emissions inventories (e.g, Kopacz et al., 2010). AQ systems mostly rely on surface observations to provide analyses as is done by the French air quality forecasting and monitoring system, Prev'air (Honoré et al., 2008). Increased use of satellite observations (notably from GEO platforms) by AQ forcasting systems is expected to improve their performance, with benefit to society.

In this paper, we describe a thermal infrared (TIR) instrument proposed for embarkation onboard a GEO platform (called GEO-TIR), optimized for monitoring O_3 and CO in the LmT for AQ purposes. Tools used for modelling radiative transfer and performing the retrieval of atmospheric state variables from remote measurements are described in Section 2. Section 3 assesses the vertical sensitivity of the proposed instrument to atmospheric state variables relevant to AQ, and provides estimates of retrieval errors. We assess the added value of a GEO instrument dedicated to monitoring the LmT (GEO-TIR) compared to an instrument measuring in the same bands but with characteristics primarily optimized for temperature and humidity (GEO-TIR2), with particular emphasis on the capability to monitor O_3 and CO in the LmT. Retrieval studies are performed for several typical European atmospheric composition profiles to characterize the instrument configuration, and over atmospheric composition profiles covering Europe during summer to provide assessment of the instrument vertical capabilities for a realistic atmosphere simulated by a state-of-the-art Chemistry Transport Model (CTM). Section 4 summarizes results and presents conclusions.

2 Retrieval of O_3 and CO

2.1 The forward model

The forward model KOPRA (Karlsruhe Optimized and Precise Radiative transfer Algorithm) is used to simulate the spectra measured by the proposed GEO-TIR instrument. KOPRA (Stiller et al., 2002) is a fast line-by-line code especially developed for analysis of data measured by high resolution interferometers. KOPRA was originally developed for the retrieval of spectra from the MIPAS (Michelson Interferometer for Passive Atmospheric Sounding) instrument onboard ENVISAT (Fischer et al., 2008). Recently it has been applied to the analysis of spectra measured from IASI on METOP-A (Eremenko et al., 2008).

Parallel to the forward calculation, KOPRA determines analytically the derivatives of the spectrum with respect to atmospheric and instrument retrieval parameters, namely the Jacobians (Höpfner et al., 1998). The KOPRA spectroscopic parameters are from the MIPAS database (Flaud et al., 2003) for O_3 and HITRAN 2004 (Rothman et al., 2005) for other species. High resolution atmospheric radiance spectra have been generated for cloud-free and aerosol-free conditions. Continua for carbon dioxide (Cousin et al., 1985) and water vapour (Clough, 1995) are also included.

2.2 Retrieval scheme

By using the analytical derivatives of the spectral signal with respect to the atmospheric state, a retrieval code was built around KOPRA. The retrieval code supports the simultaneous analysis of multiple spectral microwindows and various retrieval schemes. For the present analysis, the Tikhonov-Phillips regularization is employed (Tikhonov, 1963; Phillips, 1962):

$$\boldsymbol{x}_{i+1} = \boldsymbol{x}_i + (\boldsymbol{K}_i^T \boldsymbol{S}_y^{-1} \boldsymbol{K}_i + \gamma \boldsymbol{L}^T \boldsymbol{L})^{-1} \left[\boldsymbol{K}_i^T \boldsymbol{S}_y^{-1} (\boldsymbol{y} - \boldsymbol{F}(\boldsymbol{x}_i)) - \gamma \boldsymbol{L}^T \boldsymbol{L} (\boldsymbol{x}_i - \boldsymbol{x}_a) \right] \quad (1)$$

where $\boldsymbol{i}$ is the index on the iterations, $\boldsymbol{x}$ is the vector of atmospheric state variables to be retrieved, $\boldsymbol{x}_a$ is the a priori profile, $\boldsymbol{y}$ is the vector of the measured spectral radiances, $\boldsymbol{K}$ is the matrix of the partial derivatives of spectral radiances with respect to the atmospheric state variables, $\boldsymbol{S}_y$ is the measurement error covariance matrix, $\boldsymbol{F}$ represents the nonlinear forward model KOPRA, γ is a scalar user-defined regularization parameter, and $\boldsymbol{L}$ is a first order finite differences matrix; the T superscript represents the transpose. As commonly done, the regularization parameter γ is chosen to be as small as possible and adjusted empirically to avoid oscillations in the vertical profiles. The retrieval is performed from 0 to 39 km with a vertical step of 1 km; above 39 km the radiative transfer model and the retrieval scheme use a climatology. The state vector used in the retrieval scheme is the natural logarithm of the volume mixing ratio (VMR) values. The O_3 and CO a priori profiles are an average over Europe during northern summer calculated with the CTM MOCAGE (MOdèle de Chimie Atmospherique à Grande Echelle, Peuch et al. (1999)), over Europe during summer and are presented in Figure 1 along with the standard deviation of the mean. In the troposphere, for

both O_3 and CO, the standard deviation is high near the surface, low in the free troposphere and increases in the upper troposphere. The shape of the CO and O_3 profiles is standard for European summer conditions: the maximum of CO is located at the surface and the concentration decreases with altitude; for O_3 the opposite is the case. In this study, the a priori profile is kept constant in the horizontal and in time to help distinguish between information provided by the measurement and by the a priori.

2.3 Error budget

A linear approach is used to estimate the total error on the retrieved products. The resulting total error consists of the following: the measurement error, the model parameters error and the smoothing error (Rodgers, 2000).

The retrieval noise $\boldsymbol{S}_n$ is the mapping of the measurement noise $\boldsymbol{S}_y$ onto the retrieval. Its error covariance matrix is calculated as:

$$\boldsymbol{S}_n = \boldsymbol{G}_y \boldsymbol{S}_y \boldsymbol{G}_y^T \tag{2}$$

where $\boldsymbol{G}_y$ is the gain matrix defined as:

$$\boldsymbol{G}_y = (\boldsymbol{K}^T S_y \boldsymbol{K} + \gamma \boldsymbol{L}^T \boldsymbol{L})^{-1} \boldsymbol{K}^T \boldsymbol{S}_y^{-1}. \tag{3}$$

The model parameters error $\boldsymbol{S}_p$ represents the uncertainty of parameters used in the radiative transfer simulation. The error covariance matrix for this contribution is:

$$\boldsymbol{S}_p = \boldsymbol{G}_y \boldsymbol{K}_b \boldsymbol{S}_b \boldsymbol{K}_b^T \boldsymbol{G}_y^T \tag{4}$$

where $\boldsymbol{S}_b$ is the error covariance matrix representing uncertainty of the parameters $\boldsymbol{b}$, for example interfering species or temperature. $\boldsymbol{K}_b$ represents the Jacobians with respect to these parameters.

The smoothing error represents the error due to the limited vertical resolution of the retrieval. The error covariance matrix of the smoothing error can be expressed as:

$$\boldsymbol{S}_s = (\boldsymbol{A} - \boldsymbol{I}) \boldsymbol{S}_e (\boldsymbol{A} - \boldsymbol{I})^T \tag{5}$$

where $\boldsymbol{I}$ is the identity matrix, $\boldsymbol{S}_e$ is the error covariance matrix of an ensemble of states which describes the variability of the atmosphere. $\boldsymbol{A}$ is the averaging kernels matrix (AVK) representing the sensitivity of the retrieval to the true state, calculated as:

$$\boldsymbol{A} = \boldsymbol{G}_y \boldsymbol{K} = (\boldsymbol{K}^T S_y \boldsymbol{K} + \gamma \boldsymbol{L}^T \boldsymbol{L})^{-1} \boldsymbol{K}^T \boldsymbol{S}_y^{-1} \boldsymbol{K}. \tag{6}$$

The total error covariance matrix is given by:

$$\boldsymbol{S}_x = \boldsymbol{S}_n + \boldsymbol{S}_p + \boldsymbol{S}_s. \tag{7}$$

The errors described and discussed in this study correspond to the square roots of the diagonal elements of the calculated covariance matrices. The error is assumed unbiased, and is simulated randomly using a normal distribution.

2.4 Instrument configurations

The instrument configurations simulated in this study differ only by their Signal to Noise Ratio (SNR) and their Spectral Sampling Interval (SSI). The SNR is calculated for a surface temperature of 280 K. The noise is simulated with a Gaussian distribution with a root-mean square (RMS) equal to the Noise Equivalent Spectral Radiance (NESR). The SSI is calculated as SSI=1/(2*OPDmax), where OPDmax is the maximum optical path difference for an Fourier Transform Spectrometers (FTS).

All the other parameters are identical for all the instrument configurations:

- The pixel size is $0.5° \times 0.5°$, which corresponds to the mesh size of the AQ model we use.
- The field of view over Europe is between 32° N and 72° N and between 16° W and 36° E.
- The observation frequency is 1 hour.
- The spectral window for O_3 is taken between 1000 cm^{-1} to 1070 cm^{-1} and the one for CO is taken between 2085 cm^{-1} and 2185 cm^{-1}.
- They use the same apriori and regularization parameter (γ): 1e3 for CO and 1e4 for O_3

The objective is to evaluate the impact of the SNR and the SSI on the instrument sensitivity to O_3 and CO in the LmT, and to select a particular configuration for AQ purposes.

3 Infrared instrument capabilities for O_3 and CO

Remote sensing from space in the TIR band has shown its value in the study of atmospheric chemistry (Clerbaux et al., 2003, and references therein). Tropospheric observations from LEO platforms have already demonstrated the potential for detecting constituents relevant for AQ. For example, Clerbaux et al. (2008b) demonstrate that the CO pollution arising from large cities and urban areas can be distinguished from the background transported pollution using MOPITT thermal IR retrievals during daytime and at locations where the thermal contrast (temperature at surface minus air temperature near the surface) is significant. A study over the Indian subcontinent from Kar et al. (2008) also shows that MOPITT provides information on LmT CO in selected continental regions with strong thermal contrast and could be useful for pollution studies. Dufour et al. (2010) present the capability of IASI to probe seasonal and day-to-day variations of lower tropospheric ozone on the regional scales of highly populated areas. Kar et al. (2010) show the possibility of detecting an urban signature in the tropospheric column ozone data derived from TOMS (Total Ozone Mapping Spectrometer) and OMI satellite data. Shim et al. (2009) discuss the spatial and day-to-day variability of TES O_3 and compare this to in situ data over the Mexico City Metropolitan Area at 600–800 hPa. However, the main caveat of LEO satellites is their daily revisit time which does not allow them

to observe the diurnal variability of atmospheric constituents. As a consequence, the only practical approach to observe atmospheric composition from space with a revisit time appropriate to the time scale of pollutants ($\sim$ 1 hour) is from a geostationary orbit (Edwards, 2006).

3.1 Optimum instrument characteristics onboard a Geostationary Platform

Currently, six LEO instruments provide CO and/or O_3 observations from the IR thermal band; four from a nadir viewing platform: MOPITT (Drummond and Mand, 1996a) launched in 1999, AIRS (Aumann et al., 2003) lauched in 2002, TES (Beer, 2006) launched in 2004 and IASI (Clerbaux et al., 2009) launched in 2006 and 2 from a limb–viewing platform: MIPAS (Michelson Interferometer for Passive Atmospheric Sounding) (Fischer et al., 2008) launched in 2002 and ACE (Atmospheric Chemistry Experiment) (Bernath et al., 2005) launched in 2003. All these instruments are based upon FTS, except MOPITT and AIRS which are a gas correlation radiometer and a grating spectrometer, respectively. The spectral sampling interval (SSI) of the FTS instruments varies from 0.02 cm^{-1} for ACE to 0.25 cm^{-1} for IASI. Recently, a study has been done to monitor pollution in the lower troposphere from a drifting orbit with a Static Infrared Fourier Transform Interferometer (SIFTI), (Pierangelo et al., 2008). SIFTI is defined with a SSI of 0.0625 cm^{-1} and a NESR of 9.7 nW/(cm^2.sr.cm^{-1}) in the O_3 spectral band and 0.91 nW/(cm^2.sr.cm^{-1}) in the CO spectral band.

In this study, we define an "optimum" instrument in the TIR band with a SSI and a Signal to Noise Ratio (SNR) chosen to obtain a maximum degree of freedom (DOF) in the troposphere (0-15 km). The DOF is calculated as the trace of the AVK (Rodgers, 2000) and has been obtained for an idealized case where all the parameters (see section 2.4) are fixed except the SNR and SSI. Note that the DOFs depend on the instrument configuration but also on the a priori and the retrieval method, which in this study is the Tikhonov-Phillips regularization. For this idealized study, we retrieve two typical CO and O_3 profiles over Europe, representative of a positive and a negative thermal contrast.

In Figures 2 and 3, different DOF values have been obtained as a function of the SNR and the SSI of various TIR instruments. SNRs are taken between 50 and 3000 which correspond approximately to a NESR between 4.5 and 90 nW/(cm^2.sr.cm^{-1}) for the O_3 band and between 0.06 and 3.8 nW/(cm^2.sr.cm^{-1}) for the CO band. SSIs are taken between 0.025 cm^{-1} and 1 cm^{-1} to cover a wide range of potential instrument configurations. In this idealized study, only the measurement noise and the smoothing error (assumed to be the dominant errors) are considered since it is not straightforward to adjust the regularization parameter to minimize the total error for the 42 instrument configurations arising from different SSI and SNR values. Two cases have been considered depending on a positive thermal contrast (+2 K Figures 2a and 3a) and a negative thermal contrast (-2 K Figures 2b and 3b). This accounts for the known dependence of the O_3 and CO retrieval on the thermal contrast for TIR measurements. For example, Deeter et al. (2007) show that the sensitivity of MOPITT observations to CO concentrations in the lower troposphere varies widely as a result of variability in thermal contrast conditions. Landgraf and Hasekamp (2007) demonstrate using simu-

lated radiances from TES that a positive thermal contrast enhances O_3 sensitivity close to the surface and reduces sensitivity at higher altitudes. For a positive thermal contrast (Figure 2), the DOFs for heights below 15 km vary between 0.4 for the worst case (SNR=50 and SSI=3.2 cm^{-1}) and 2.3 for the best case (SNR=3000 and SSI=0.025) for O_3; and between 0.9 to 4.8 for CO. For the negative thermal contrast (Figure 3), the DOFs vary from 0.35 to 2.15 for O_3 and from 0.9 to 3.5 for CO.

For AQ purposes, the main interest is to have a maximum of information in the LmT, documenting residual layers that are capable of mixing with the planetary boundary layer (PBL). Considering current IR instruments, technical feasibility and cost (Astrium-EADS, personal communication) a DOF of $\sim$1.5 for O_3 and of $\sim$2 for CO seems to be a good compromise to have vertical information in the troposphere. Considering characteristic values of DOFs providing information on O_3 and CO in the LmT (DOF=1.5 and 2, respectively), several pairs of (SNR, SSI) depending on the instrument concept (e.g. FTS, grating spectrometer), can be envisaged. In this idealized study, we select one configuration compatible for a FTS instrument (Table 1). However, on Figures 2 and 3, we see that different SNR and SSI values can provide the same DOF; for instance a higher SSI allows to relax the SNR requirement. For this reason, the results hereinafter presented with the chosen (SNR, SSI) pair do not depend on the instrument concept; they only depend on the SNR and SSI. For these specific configurations, the spectral microwindows have been selected according to a previous study on IASI (Clerbaux et al., 1998; Turquety et al., 2004) to avoid contamination by other species. The smoothing error, the measurement error and the temperature error are considered for these specific configurations. The contributions of the surface properties (surface temperature and emissivity) are not taken into account since they are low (e.g, Clerbaux et al., 2008a; Boynard et al., 2009) compared to other components (e.g., smoothing error). Note that the SSI and SNR selected for GEO-TIR are equivalent to the ones chosen for the TIR sensor of MAGEAQ (Peuch et al., 2010). However, GEO-TIR does not simulate the full MAGEAQ instrument since we do not consider the visible band nor the spatial resolution, which is $\sim$ 15 km (goal) for MAGEAQ. Instead, we consider a pixel size of $\sim$ 50 km for GEO-TIR. Because this study focuses on providing a first estimate of the capabilities of GEO-TIR in the LmT, this is appropriate.

Figures 4a and 4b present the AVKs for O_3 for a thermal contrast equal to 0 K corresponding to a SNR=750 and a SSI=0.05 cm^{-1} and its corresponding error budget, respectively. The AVKs are calculated from 0 to 39 km with 1 km of vertical resolution but plotted from 0 to 20 km to focus on the troposphere and to show the full shape of the AVKs corresponding to the levels in the LmT. The lowermost maximum of the AVKs is located at 5 km, above the PBL which is situated at 1-2 km at noon in summer. The DOF obtained for heights below 15 km is 1.5. Figure 4b presents the different main components of the total error: measurement, temperature, smoothing and a priori errors. Given current absolute uncertainty in temperature observations, which is around 1 K for IASI (Pougatchev et al., 2009), an improvement up to a total uncertainty of 0.5 K will likely be achieved by combining the next generation satellite products like MTG-IRS and contemporary meteorological

analyses systems. Thus, we considered a temperature uncertainty of 0.5 K at each vertical level. Such an assumption was made in Clerbaux et al. (2008a). The temperature and measurement errors on the retrieved profile are low (less than 5%). The most important error is the smoothing error which is superimposed with the total error in Figure 4b. At the surface, the total error (50%) is slightly lower than the a priori error (57%). In the same way, at altitudes of 2 and 3 km, namely at the top of the PBL or just above, the total error is lower than the a priori error: 15% instead of 30%, and 12% instead of 25%, respectively.

Figures 5a and 5b present the same results but for CO with SSI=0.05 cm^{-1} and SNR=190. The lower maximum of the AVK is located at 3 km and the DOF obtained for heights below 15 km is $\sim$2. The temperature error is larger than for O_3 and can reach 5% at the surface. The measurement error (around 2%) is still low compared to other error components. At the surface, at 2 km and 3 km in altitude the total error is always lower than the a priori error: 20%, 8% and 6% instead of 25% 11% and 10%, respectively.

As for AQ purposes we are interested in monitoring the LmT, we plot in Figure 6 the AVKs at the surface for CO and O_3 as a function of the thermal contrast from -10 K to 10 K to quantify the vertical information content of GEO-TIR in the LmT. We also simulate AVKs from another TIR instrument onboard a GEO platform, referred to as GEO-TIR2, using the SNR and SSI of the Meteosat Third Generation InfraRed Sounder (MTG-IRS) (Stuhlmann et al., 2005), which is dedicated to NWP (temperature and humidity). It has a SSI of 0.625 cm^{-1} for both O_3 and CO, and a NESR of 6.12 nW/(cm^2.sr.cm^{-1}) and 24.5 nW/(cm^2.sr.cm^{-1}) for the CO and O_3 spectral windows, respectively (Clerbaux et al., 2008a). These noise values correspond to an SNR of 30 and 185 for CO and O_3, respectively, for a surface temperature of 280 K (Table 1). As GEO-TIR for MAGEAQ, GEO-TIR2 does not simulate the full MTG-IRS mission since we consider a pixel size $\sim$ 50 km for GEO-TIR2 (limited by the model mesh) instead of $\sim$ 4 km for MTG-IRS and a revisit time of 1 hour which is at the upper limit of the MTG-IRS capability. However, the relative comparison of GEO-TIR and GEO-TIR2 provides a reasonably accurate first order estimate of the vertical added value in the LmT of GEO-TIR compared to GEO-TIR2. For CO (Figure 6) with high positive thermal contrast (10 K), GEO-TIR can be sensitive at 1 km whereas for negative thermal contrast it is sensitive at 5 km and above. GEO-TIR2 is also sensitive in the LmT for CO for high positive thermal contrast, but the AVK values are low (AVKs < 0.1) compared to GEO-TIR, for which values can reach 0.23. Concerning O_3, GEO-TIR is less sensitive than for CO in the LmT. However, with high positive thermal contrast AVKs for O_3 can reach 0.15 at 3 km in altitude. GEO-TIR2 presents very low sensitivity in the LmT (AVKs < 0.04) even with high positive thermal contrast.

These results show that a nadir instrument with the characteristics described in this section (GEO-TIR) can add information on O_3 and CO concentrations in the LmT compared to an instrument not optimized for AQ (GEO-TIR2). However, both GEO instruments have generally little information at the surface. Such information may be provided at particular locations by surface observations

from European AQ networks. Studying the complementarity of a GEO and surface AQ networks is a useful exercise, but outside the scope of this paper.

3.2 Geostationary observation system

To go a step further in our analysis, we simulate CO and O_3 retrieved profiles over Europe during summer, to better characterize the vertical added value of a TIR instrument to monitor the LmT for a realistic atmosphere and not only for typical profiles as was done in section 3.1. To study this added value, we first simulate the CO and O_3 observations from both platforms by sampling the atmosphere using the MOCAGE model (Peuch et al., 1999), a state-of-the-art three-dimensional CTM from Météo-France. MOCAGE simulates interactions between dynamical, physical and chemical processes in the troposphere and in the stratosphere. Its vertical resolution is 47 hybrid levels from the surface up to 5 hPa with a resolution of about 150 m in the LmT increasing to 800 m in the upper troposphere. MOCAGE is used for several applications: chemical weather forecasting at Météo-France (Dufour et al., 2004) and data assimilation research (e.g., El Amraoui et al., 2008, 2010). MOCAGE is also used in the operational AQ monitoring system in France: Prev'air (Rouïl et al., 2008) and in the pre-operational GMES atmosphere core service (Hollingsworth et al., 2008). In this study, we consider the European domain with a horizontal resolution of $0.5° \times 0.5°$. The MOCAGE run which we sample is termed the nature run. We considered an error on the temperature profile of 0.5 K for both instruments (GEO-TIR and GEO-TIR2).

After sampling the atmosphere using MOCAGE (see above), the forward model KOPRA is used to generate corresponding atmospheric radiances seen by GEO-TIR and GEO-TIR2; these include representative values of SSI and noise on the signal. After producing these radiances, the KOPRA-fit retrieval scheme is used to produce CO and O_3 profiles for GEO-TIR and GEO-TIR2. To account for cloudy scenes, cloud estimates from the ARPEGE meteorogical analysis (Courtier et al., 1991) are used to assign cloud fraction to the observation pixels. Pixels with a cloud fraction greater than 0.5 are filtered out, accounting for cloud coverage over Europe. Taken together, the different steps used to produce these CO and O_3 observations (see above) are termed the geostationary observation system (GOS).

Considering the high computational burden of such simulations, we select a day in summer, namely July 12^{th}, 2009, representative of a typical northern summer day, with no meteorological or pollution major event, to simulate observations from both satellites over Europe. The meteorological situation for July 12^{th}, 2009, shows an anticyclone over the Mediterranean sea and a low-pressure area over the North West of Ireland which generates a westerly wind flow over Western Europe. That day was cloudy over Northern Europe and clear over the Mediterranean Basin which leads to a European-wide cloud cover of 50%, which is represented in Figure 7 by the grey area. Figure 7 represents the surface temperature and the thermal contrast at 0h UTC and at 12h UTC on July 12^{th}, 2009 from the ARPEGE model. During night, low surface temperature and negative thermal contrast

are observed over land (the latter can reach -8 K over France), whereas during daytime high surface temperature and positive thermal contrast are observed (the latter can reach 15 K over Spain or North Africa). Over sea the thermal contrast is close to 0 K or slightly positive. In this study, the emissivity is equal to unity. This slightly overestimates the impact of the thermal constrast. However, since we use the same thermal constrast and emissivity for GEO-TIR and GEO-TIR2, the relative comparison between these instruments should be meaningful.

3.3 Comparison of geostationary thermal infrared observations of O_3 and CO

3.3.1 Spatial distributions of retrieved O_3 and CO

Figure 8 presents O_3 concentrations at 3 km on July 12^{th}, 2009 during nighttime (00h UTC) and daytime (12h UTC) simulated by MOCAGE (the nature run), and simulated by the GOS for GEO-TIR and GEO-TIR2. The grey area corresponds to pixels with more than 50% cloud-fraction, where retrievals are not done. MOCAGE CO and O_3 fields have not been smoothed by GEO-TIR and GEO-TIR2 AVKs in order to represent the total error (see section 2.3) in the comparison with both satellites. In the nature run (Figures 8c and f) maxima of O_3 are observed over the Atlantic Ocean and France and are moving from West to East. The main spatial patterns of O_3 are represented well by GEO-TIR (Figures 8a and 8d) with a minimum of O_3 concentrations over North West Spain, North Africa and North East Iceland. The maxima are also well represented over Spain and over the Mediterranean Sea. However Figures 8g and 8i show that the differences (total error) between the nature run and GEO-TIR range between -40% (over land) and 70% (over sea). Globally, GEO-TIR O_3 concentrations are smooth compared to the nature run: GEO-TIR minima are higher in magnitude than the nature run ones and GEO-TIR maxima are lower in magnitude than the nature run ones. Over France during nighttime, GEO-TIR does not capture the maxima of the O_3 concentrations, whereas during daytime, it captures well the maxima over Spain. Figures 8b, 8e, 8h and 8j, representing the O_3 concentrations from GEO-TIR2 and the relative differences from the nature run, show a latitudinal gradient which suggests that GEO-TIR2 is more sensitive to the upper layers of the atmosphere (strong vertical correlation in the covariance matrix S_x, where the latitudinal gradient of O_3 is strong and is contaminated by the a priori information in the LmT.

Figures 9a and 9b represent the DOFs between 0 and 3 km obtained for GEO-TIR for O_3 over the same period studied previously, July 12^{th}, 2009. The DOFs are between 0.3 and 0.85 depending on the thermal contrast and surface temperature (Figure 7). Over the land, during daytime and with a high positive thermal contrast and high surface temperature, the DOFs are high ($\sim$0.8) whereas during nighttime, with a negative thermal contrast and low surface temperature, they are low ($\sim$0.3). Over the sea, where the thermal contrast is less sensitive to the diurnal variation (Figure 7), the DOFs are about 0.5 both during daytime and nighttime. Figures 9c and 9d represent the DOFs for

GEO-TIR2. Similar remarks as for GEO-TIR can be made regarding the evolution of the DOFs with the thermal contrast and the surface temperature but the values are between 0.02 and 0.3. Figures 9e, 9f and 9g, 9h, represent the peak altitude of the lowermost AVKs of the retrieved O_3 from GEO-TIR and GEO-TIR2, respectively. This diagnostic is used to determine the vertical sensitivity of the instrument to the LmT. Over land, GEO-TIR is sensitive for O_3 around 2 km during daytime and at 4 km during nighttime whereas GEO-TIR2 is sensitive for O_3 at 14 km during daytime and at 16 km during nighttime. Over sea, the lowermost maximum of the AVKs from GEO-TIR is between 2 and 7 km and for GEO-TIR2 is between 14 and 17 km. Figures 9g and 9h confirm that GEO-TIR2 is mainly sensitive for O_3 in the upper troposphere and lower stratosphere, which is in agreement with the latitudinal gradient of O_3 concentrations observed in Figures 8e, 8f and results found in section 3.1. The difference between GEO-TIR2 and the nature run can reach 140% (e.g., over the Atlantic ocean).

Figure 10 presents CO concentrations at 3 km on July 12^{th}, 2009 during nighttime (00h UTC) and daytime (12h UTC) simulated by the nature run and simulated with the GOS for GEO-TIR and GEO-TIR2. In the nature run (Figures 10c and f), maxima of CO are observed over the Atlantic Ocean, Western Spain and Italy and minima are observed over the Atlantic Ocean. Figures 10a and 10b show that CO observations from GEO-TIR are close to the nature run (Figures 10c and 10f). They present maxima over North West Spain, in the Mediterranean Sea near Sardinia and Sicily and over Italy. The minima are also well represented over North East Iceland, over South West Spain and over the South East Mediterranean Basin. Figures 10g and 10i show that the differences between GEO-TIR and the nature run are between -25% and 30% for CO and are lower in magnitude than for O_3. However, GEO-TIR CO concentrations are smoother compared to the nature run ones (GEO-TIR minima in magnitude are higher than the nature run ones and GEO-TIR maxima in magnitude are lower than the nature run ones). Figures 10b, 10e, 10h and 10j present similar results for GEO-TIR2. In opposition to the GEO-TIR2 O_3 results, GEO-TIR2 is able to capture some CO horizontal spatial patterns over North East Iceland and over North West Spain. However, the maxima of CO concentrations in GEO-TIR2 observations over the South East Mediterranean Basin are not comparable in magnitude with those of the MOCAGE nature run at 3 km of altitude. Similar maxima are observed in the nature run around 11 km (not shown) which may indicate that GEO-TIR2 observations of CO at 3 km can be affected by higher CO concentrations at higher levels in altitude. The differences between GEO-TIR2 and the nature run for CO are between -30% and 70%.

Figures 11a and 11b show that the DOFs for CO between 0 and 3 km obtained for GEO-TIR are between 0.4 (over sea) and 1 (over land during daytime) and Figures 11c and 11d indicate that the DOFs obtained for GEO-TIR2 CO range between 0.2 and 0.5. Figures 11e and 11f show that GEO-TIR is sensitive for CO at 1 km during daytime over land and between 3 and 4 km over sea and during nighttime. Figures 11g and 11h show that GEO-TIR2 is sensitive for CO at the altitude of 1 km over particular locations where there is very high positive thermal contrast. However, it is

generally sensitive between 5 and 6 km of altitude. The DOF between 0-15 km is ~ 1 (not shown) which means that GEO-TIR2 can monitor the tropospheric CO column as presented by Clerbaux et al. (2004, 2008a). CO maxima can be detected when they are located in the lower troposphere with high positive thermal contrast, whereas when the CO maxima are located in the middle or upper troposphere (e.g. due to long range transport) GEO-TIR2 is sensitive to this maximum CO value and not to CO in the LmT. These results confirm that the thermal contrast and the surface temperature affect both GEO-TIR2 and GEO-TIR observations of CO and O_3. Both satellites provide better results in the troposphere for CO than for O_3 since higher concentrations of CO are located in the troposphere whereas higher concentrations of O_3 are located in the stratosphere.

3.3.2 Time-series of retrieved O_3 and CO

In order to better represent the capabilities of GEO-TIR to capture the LmT variability for O_3 and CO, Figure 12 shows the time-series of the 0-3 km columns of O_3 and CO over these 6 European cities: Amsterdam, Berlin, London, Madrid, Paris and Rome for the nature run, GEO-TIR and GEO-TIR2. Figure 13 presents the time-series of surface temperature and thermal contrast over 6 European cities. Tables 2 and 3 present the correlation, the bias and the standard deviation for O_3 and CO between the nature run and GEO-TIR, and the nature run and GEO-TIR2 for 0-3 km and 0-6 km columns for these 6 cities. At the beginning of the period: from July 1^{st} to July 4^{th}, GEO-TIR is able to capture well the maximum observed in the O_3 columns over all 6 cities. GEO-TIR is also able to represent well the minimum observed on July 11^{th}, 2009 over London. In the same way, over Madrid, GEO-TIR captures the diurnal variability, especially from July 7^{th}, 2009 to July 12^{th}, 2009. This period corresponds to high positive thermal contrast with high surface temperature over Madrid, and high PBL depth with an increase of O_3 concentrations during the day seen by GEO-TIR. However, except over Madrid and Rome, GEO-TIR tends to overestimate O_3 concentrations between July 8^{th}, 2009 and July 12^{th}, 2009. This period corresponds to low or negative thermal contrasts and low surface temperatures, so that GEO-TIR is less sensitive to the LmT. In these conditions, the retrieved profiles are more contaminated by the a priori through the retrieval process. Table 2 shows that the correlation for the O_3 0-3 km column between the nature run and GEO-TIR is between 0.71 and 0.81 and between 0.74 and 0.92 for the O_3 0-6 km column, which indicates good monitoring capabilities for the GEO-TIR in the LmT. The bias between GEO-TIR and the nature run is mainly positive for the 0-3 and 0-6 km columns which reflects the overestimation of O_3 concentrations observed in Figure 12. The standard deviation of the differences between GEO-TIR and the nature run is $\sim$12% for the O_3 0-3 km column and $\sim$8% for the O_3 0-6 km column. As opposed to GEO-TIR, Figure 12 and Table 2 show that GEO-TIR2 has very low sensitivity to O_3 in the LmT.

As for O_3, GEO-TIR represents well the diurnal variability, the maxima and the minima over all 6 cities for the CO 0-3 km column (Figure 12). This indicates that even with low thermal contrast

GEO-TIR is able to capture the variability of the CO 0-3 km column. The bias between GEO-TIR and the nature run is mainly negative ($\sim$6% for the CO 0-3 km column and $\sim$4% for the CO 0-6 km column) over all the 6 cities since GEO-TIR captures the maxima of CO but with an underestimation. This is because the maximum values of CO in the nature run are located in the layer near the surface (0-500m) where GEO-TIR is less sensitive. The standard deviation is $\sim$6% for the CO 0-3 km column and $\sim$4% for the CO 0-6 km column. The correlation between the nature run and GEO-TIR is between 0.79 and 0.90 for the CO 0-3km column and between 0.85 and 0.91 for the CO 0-6km column. Figure 12 and Table 2 also show that GEO-TIR2 presents better results in the LmT for CO than for O_3 as explained previously in section 3.3.1. The correlation between GEO-TIR2 and the nature run for the CO 0-3 km column, is between 0.39 and 0.74 and between 0.52 and 0.85 for the CO 0-6 km columns. Agreement between GEO-TIR and the nature run is better than that between GEO-TIR2 and the nature run, as evidenced by the higher correlations for the former comparison. This shows the capabilities of GEO-TIR to measure O_3 and CO in the LmT, and its added value with respect to GEO-TIR2.

4 Summary and Conclusions

In this paper, we perform retrieval studies to evaluate the vertical capability of a nadir TIR sensor with high SNR and SSI, onboard a geostationary platform, for monitoring O_3 and CO in the lowermost troposphere (LmT; 0-3 km) over Europe. For simulated O_3 and CO profiles, we calculate the DOFs for different instrument configurations (SNR and SSI) for a positive (+2 K) and negative (-2 K) thermal contrast for an idealized case, considering all the parameters (e.g., regularization) fixed except the SSI and the SNR. We note that several instrument configurations can lead to the same DOF (a low SSI with a high SNR can be equivalent to a high SSI with a low SNR). From these results, we select a particular instrument configuration that is technically achievable (SSI=0.05 cm^{-1} and SNR=750 for O_3; SSI=0.5 cm^{-1} and SNR=190 for CO), called GEO-TIR, and simulate the main error components (smoothing error, measurement error and temperature error). For O_3 and CO, we find that an instrument with these characteristics can provide information in the LmT. At an altitude of 2 km, the total error is lower than the a priori error: 15% instead of 30% for O_3 and 8% i nstead of 11% for CO.

MTG-IRS is a nadir TIR sensor which is planned to be onboard a geostationary platform, and will be dedicated to measure temperature and humidity. However, as MTG-IRS will be launched in the 2016-2018 timeframe and will measure radiances in the CO and O_3 TIR bands, we simulate an infrared geostationary instrument (GEO-TIR2) with SNR and SSI similar to MTG-IRS to quantify the vertical added value of a nadir TIR sensor complementing the air quality (AQ) observing system (GEO-TIR). To better characterize the vertical information provided by GEO-TIR and GEO-TIR2 in the LmT, we retrieve two typical profiles of O_3 and CO for different thermal contrast, positive and

negative. The shape of the first averaging kernel (corresponding to the surface level) confirms that GEO-TIR shows good sensitivity for CO in the LmT and for O_3 for high positive thermal contrast. However, GEO-TIR2 shows very low sensitivity in the LmT for O_3 but can be sensitive with high positive thermal contrast for CO.

Ozone and CO distributions over Europe as measured by GEO-TIR and the GEO-TIR2 are simulated. This is done using results of the 3D CTM MOCAGE coupled with a radiative transfer model KOPRA and its associated retrieval scheme KOPRA-fit. The simulation of spatial variability during nighttime and daytime of GEO-TIR observations shows that GEO-TIR simulates well the horizontal O_3 and CO spatial patterns at 3 km compared to the nature run provided by MOCAGE. The maxima and minima in magnitude are generally well detected but smoother compared to those in the nature run. The DOFs calculated for 0-3 km are between 0.3 and 0.85 for O_3 and between 0.4 and 1 for CO, depending on the surface thermal contrast. Conversely, GEO-TIR2 shows very low sensitivity to the O_3 in the LmT and the concentrations at 3 km reflect the O_3 latitudinal gradient observed in the upper layers of the troposphere. The DOFs obtained for CO in the troposphere is around 1 which indicates that GEO-TIR2 is sensitive to the CO tropospheric column, and range between 0.2 and 0.5 for the 0-3 km column. In the case of high positive thermal contrast and high surface temperature, GEO-TIR2 has sensitivity to CO in the LmT. However, it is difficult to discriminate CO in the middle or upper troposphere and CO in the LmT, because GEO-TIR2 has just CO column information (DOF$\sim$1). Simulations of the temporal evolution of the 0-3 km column show that GEO-TIR is able to capture well the variability in O_3 and CO and the diurnal cycle with high positive thermal contrast and high surface temperature. The correlation between GEO-TIR and the nature run is between 0.71 and 0.81 for O_3 (0-3 km column) and between 0.79 and 0.90 for CO (0-3 km column). Concerning GEO-TIR2, it presents very low sensitivity to the O_3 concentration in the LmT and some sensitivity to CO concentrations with favourable conditions (e.g. high concentration in the LmT and high positive thermal contrast). The correlations between the nature run and GEO-TIR2 are lower than the GEO-TIR ones.

These results show that a nadir TIR sensor onboard a GEO platform with a specific instrument configuration (high SNR and SSI) is sensitive to the LmT especially for positive thermal constrast and high surface temperature (typically over land during daytime) for both CO and O_3. We have shown that such a configuration (GEO-TIR) is capable of bringing added value in the LmT compared to a configuration optimized for numerical weather prediction (GEO-TIR2). In a subsequent study, we will perform observing system simulation experiments (OSSEs) to further quantify the impact of such a satellite instrument on AQ analyses and forecasts. Future work will also concern multispectral retrievals to improve these measurements at the surface, with a methodology similar to that of Worden et al. (2007); Landgraf and Hasekamp (2007) for TES and OMI concerning TIR and the ultraviolet spectral region. In particular, adding channels in the visible (Chappuis bands) as for the MAGEAQ instrument, should improve sensitivity to O_3 concentrations in the near surface, likely

reaching between 2.5 and 3 DOFs for O_3 in the troposphere, and thus providing effective sounding capability for the LmT. For improving CO measurements at the surface, one possibility is to add a near infrared band as was done by Edwards et al. (2009) and proposed in GEO-CAPE. Regarding the relevance of the added value of GEO-TIR, such a mission could be a key part of future plans for the Global Observing System. The authors thank veru much the referees for their usefull comments that helped improve the paper.

Acknowledgements. This work was funded by the Centre National de Recherches Scientifiques (CNRS), Astrium-EADS, the Centre National de Recherches Météorologiques (CNRM) of Météo–France and the RTRA/STAE (POGEQA project). The authors acknowledge ETHER, the French atmospheric composition database (CNES and CNRS-INSU) and the Région Midi– Pyrénées (INFOAIR project).

References

Akimoto, H., Irie, H., Kasai, Y., Kanaya, Y., Kita, K., Koike, M., Kondo, Y., Nakazawa, T., and Hayashida, S.: Planning a geostationary atmospheric observation satellite, Commission on the Atmospheric Observation Satellite of the Japan Society of Atmospheric Chemistry, 2008.

Aumann, J. H., Chahine, M. T., Gautier, C., Goldberg, M. D., McMillin, E. K. L. M., Revercomb, H., Rosenkranz, P. W., Smith, W. L., Staelin, D. H., Strow, L. L., and Susskind, J.: AIRS/AMSU/HSB on the Aqua Mission: Design, Science Objectives, Data Products, and Processing Systems, IEEE Trans. Geosci. Remote Sens., 41, 253–264, 2003.

Beer, R.: TES on the aura mission: scientific objectives, measurements, and analysis overview, IEEE Trans. Geosci. Remote Sens., 44, 1102–1105, 2006.

Beer, R., Glavich, T. A., and Rider, D. M.: Tropospheric emission spectrometer for the earth observing system's Aura satellite, Applied Optics, 40, 2356–2367, 2001.

Bernath, P. F., McElroy, C. T., Abrams, M. C., Boone, C. D., Butler, M., Camy-Peyret, C., Carleer, M., Clerbaux, C., Coheur, P. F., Colin, R., DeCola, P., DeMazière, M., Drummond, J. R., Dufour, D., Evans, W. F. J., Fast, H., Fussen, D., Gilbert, K., Jennings, D. E., Llewellyn, E. J., Lowe, R. P., Mahieu, E., McConnell, J. C., McHugh, M., McLeod, S. D., Michaud, R., Midwinter, C., Nassar, R., Nichitiu, F., Nowlan, C., Rinsland, C. P., Rochon, Y., Rowlands, N., Semeniuk, K., Simon, P., Skelton, R., Sloan, J. J., Soucy, M.-A., Strong, K., Tremblay, P., Turnbull, D., Walker, K. A., Walkty, I., Wardle, D. A., Wehrle, V., Zander, R., and Zou, J.: Atmospheric Chemistry Experiment (ACE): Mission overview, Geophys. Res. Lett., 32, L15S01, doi:10.1029/2005GL022386, 2005.

Bovensmann, H., Burrows, J.-P., Buchwitz, M., Frerick, J., Noel, S., Rozanov, V. V., Chance, K. V., and Goede, A. P. H.: SCIAMACHY: Mission objectives and measurement modes, J. Atmos. Sci., 56, 127–150, 1999.

Bovensmann, H. and Orphal, J.: The geostationary component of an operational atmospheric chemistry monitoring system: Specification and expected performance, ESA Study: Operational Atmospheric Chemistry Monitoring Missions 17237/03/NL/GS (CAPACITY), 2005.

Boynard, A., Clerbaux, C., Coheur, P.-F., Hurtmans, D., Turquety, S., George, M., Hadji-Lazaro, J., Keim, C., , and Meyer-Arnek, J.: Measurements of total and tropospheric ozone from IASI:comparison with correlative satellite, ground-based and ozonesonde observations, Atmos. Chem. Phys., 9, 6255–6271, 2009.

Burrows, J. P., Bovensmann, H., Bergametti, G., Flaud, J. M., Orphal, J., Noël, S., Monks, P. S., Corlett, G. K., Goede, A. P., von Clarmann, T., Steck, T., Fischer, H., and Friedl-Vallon, F.: The geostationary tropospheric pollution explorer (GeoTROPE) mission: objectives, requirements and mission concept, Adv. Space Res., 34, 682–687, 2004.

Burrows, J. P., Weber, M., Buchwitz, M., Rozanov, V., Ladstatter-Weissenmayer, A., Richter, A., DeBeek, R., Hoogen, R., Bramstedt, K., Eichmann, K. U., and Eisinger, M.: The global ozone monitoring experiment (GOME): Mission concept and first scientific results, J. Atmos. Sci., 56, 151–175, 1999.

Callies, J., Corpaccioli, E., Eisinger, M., Hahne, A., and Lefebvre, A.: GOME-2 Metops Second-Generation Sensor for Operational Ozone Monitoring, Esa bull., No. 102, 28–36, 2000.

Clerbaux, C., Boynard, A., Clarisse, L., George, M., Hadji-Lazaro, J., Herbin, H., Hurtmans, D., Pommier, M., Turquety, A. R. S., Wespes, C., and Coheur, P.-F.: Monitoring of atmospheric composition using the thermal infrared IASI/MetOp sounder, Atmos. Chem. Phys., 9, 6041–6054, 2009.

Clerbaux, C., Chazette, P., Hadji-Lazaro, J., Mégie, G., Müller, J.-F., and Clough, S. A.: Remote sensing of CO, CH_4, and O_3 using a spaceborne nadir-viewing interferometer, J. Geophys. Res., 103(D15), 18 999–19 013, 1998.

Clerbaux, C., Coheur, P.-F., Hurtmans, D., Hadji-Lazaro, J., Turquety, S., and van Oss, R.: Capabilities of MTG-IRS to sound ozone, CO and methane using ESA pre-phase A specifications, Eumetsat EUM/CO/05/1484/SAT, 2004.

Clerbaux, C., Coheur, P.-F., Turquety, S., and Hadji-Lazaro, J.: Capabilities of infrared sounder observations for monitoring atmospheric composition and chemistry applications, Eumetsat EUM/CO/O3/1127/SAT, 2003.

Clerbaux, C., Coheur, P.-F., Scharf, O., Hurtmans, D., and Boynard, A.: The potential of MTG-IRS and S4-TIR to detect high pollution events at urban and regional scales, Eumetsat EUM/CO/07/4600000447/SAT, 2008a.

Clerbaux, C., Edwards, D. P., Deeter, M., Emmons, L., Lamarque, J.-F., Tie, X. X., Massie, S. T., and Gille, J.: Carbon monoxide pollution from cities and urban areas observed by the Terra/MOPITT mission, Geophys. Res. Lett., 35, L03817, doi:10.1029/2007GL032300, 2008b.

Clough, S. A.: The water vapor continuum and its role in remote sensing, Atmospheric and Environmental Research, Inc , Optical Remote Sensing of the Atmosphere, 22, 76–78, 1995.

Courtier, P., Freydier, C., Geleyn, J. F., Rabier, F., and Rochas, M.: The ARPEGE project at Météo France, in: Atmospheric Models, vol.2, pp. 193–231, Workshop on Numerical Methods, Reading, U.K., 1991.

Cousin, C., Doucen, R. L., Boulet, C., and Henry, A.: Temperature dependence of the absorption in the region beyond the 4.3–μm band head of CO_2. II: N_2 and O_2 broadening, Appl. Opt., 24(22), 3899–3907, 1985.

Cuvelier, C., Thunis, P., Vautard, R., Amann, M., Bessagnet, B., Bedogni, M., Berkowicz, R., Brandt, J., Brocheton, F., Builtjes, P., Carnavale, C., Coppalle, A., Denby, B., Douros, J., Graf, A., Hellmuth, O., Hodzic, A., Honoré, C., Jonson, J., Kerschbaumer, A., de Leeuw, F., Minguzzi, E., Moussiopoulos, N., Pertot, C., Peuch, V.-H., Pirovano, G., Rouïl, L., Sauter, F., Schaap, M., Stern, R., Tarrason, L., Vignati, E., Volta, M., White, L., Wind, P., and Zuber, A.: CityDelta: A model intercomparison study to explore the impact of emission reductions in European cities in 2010, Atmos.-Environ., 41, 189–207, 2007.

Deeter, M. N., Edwards, D. P., Gille, J. C., and Drummond, J. R.: Sensitivity of MOPITT observations to carbon monoxide in the lower troposphere, J. Geophys. Res., 112, D24306, doi:10.1029/2007JD008929, 2007.

Drummond, J. R. and Mand, G. S.: Evaluation of operational radiances for the Measurement of Pollution in the Troposphere (MOPITT) instrument CO thermal-band channels, J. Geophys. Res., 109, D03308, doi: 10.1029/2003JD003970, 1996a.

Drummond, J. R. and Mand, G. S.: The measurements of pollution in the troposphere (MOPITT) instrument: Overall performance and calibration requirements, J. Atmos. Oceanic Technol., 13, 314–320, 1996b.

Dufour, A., Amodei, M., Ancellet, G., and Peuch, V.-H.: Observed and modelled "chemical weather" during ESCOMPTE, Atmos. Res., 74, 161–189, 2004.

Dufour, G., Eremenko, M., Orphal, J., and Flaud, J.-M.: IASI observations of seasonal and day-to-day variations of tropospheric ozone over three highly populated areas of China: Beijing, Shanghai, and Hong Kong, Atmos. Chem. Phys., 10, 3787–3801, 2010.

Edwards, D. P.: Air Quality Remote Sensing From Space, Eos Trans. AGU, 87(33), 327, doi:10.1029/2006EO330005, 2006.

Edwards, D. P., Arellano Jr., A. F., and Deeter, M. N.: A satellite observation system simulation experiment for

carbon monoxide in the lowermost troposphere, J. Geophys. Res., 114, D14304, doi:10.1029/2008JD011375, 2009.

El Amraoui, L., Attié, J.-L., Semane, N., Claeyman, M., Peuch, V.-H., Warner, J., Ricaud, P., Cammas, J.-P., Piacentini, A., Cariolle, D., Massart, S., and Bencherif, H.: Midlatitude stratosphere–troposphere exchange as diagnosed by MLS O3 and MOPITT CO assimilated fields, Atmos. Chem. Phys., 10, 2175–2194, 2010.

El Amraoui, L., Semane, N., Peuch, V.-H., and Santee, M. L.: Investigation of dynamical processes in the polar stratospheric vortex during the unusually cold winter 2004/2005, Geophys. Res. Lett., 35, L03803, doi:10.1029/2007GL031251, 2008.

Eremenko, M., Dufour, G., Foret, G., Keim, C., Orphal, J., Beekmann, M., Bergametti, G., and Flaud, J.-M.: Tropospheric ozone distributions over Europe during the heat wave in July 2007 observed from infrared nadir spectra recorded by IASI, Geophys. Res. Lett., 35, L18805, doi:10.1029/2008GL03803, 2008.

European Space Agency (ESA): GMES Sentinels 4 and 5 Mission Requirement Document, EOP–SMA/1507, 2007.

Fischer, H., Birk, M., Blom, C., Carli, B., Carlotti, M., von Clarmann, T., Delbouille, L., Dudhia, A., Ehhalt, D., Endemann, M., Flaud, J.-M., Gessner, R., Kleinert, A., Koopman, R., Langen, J., López-Puertas, M., Mosner, P., Nett, H., Oelhaf, H., Perron, G., Remedios, J., Ridolfi, M., Stiller, G., and Zander, R.: MIPAS: an instrument for atmospheric and climate research, Atmos. Chem. Phys., 8, 2151–2188, 2008.

Flaud, J. M., Orphal, J., Bergametti, G., Deniel, C., von Clarmann, T., Friedl-Vallon, F., Steck, T., Fischer, H., Bovensmann, H., Burrows, J. P., Carlotti, M., Ridolfi, M., and Palchetti, L.: The Geostationary Fourier Imaging Spectrometer (GeoFIS) as part of the Geostationary Tropospheric Pollution Explorer (GeoTroPE) mission: objectives and capabilities, Adv. Space Res., 34, 688–693, 2004.

Flaud, J.-M., Piccolo, C., Carli, B., Perrin, A., Coudert, L. H., Teffo, J.-L., and Brown, L. R.: Molecular line parameters for the MIPAS (Michelson Interferometer for Passive Atmospheric Sounding) experiment, Atmos. Oceanic Opt., 16, 172–182, 2003.

Guerova, G., Bey, I., Attié, J.-L., Martin, R. V., Cui, J., and Sprenger, M.: Impact of transatlantic transport episodes on summertime ozone in Europe, Atmos. Chem. Phys., 6, 2057–2072, 2006.

Hollingsworth, A., Engelen, R., Textor, C., Boucher, O., Chevallier, F., Dethof, A., Elbern, H., Eskes, H., Flemming, J., Granier, C., Kaiser, J. W., Morcrette, J. J., Rayner, P., Peuch, V.-H., Rouïl, L., and the GEMS Consortium: Toward a monitoring and forecasting system for atmospheric composition: The GEMS Project, Bull. Amer. Meteor. Soc., 89, 8, 1147–1164, 2008.

Honoré, C., Rouïl, L., Vautard, R., Beekmann, M., Bessagne, B., Dufour, A., Elichegaray, C., Flaud, J.-M., Malherbe, L., Meleux, F., Menut, L., Martin, D., Peuch, A., Peuch, V.-H., and Poisson, N.: Predictability of European air quality: Assessment of 3 years of operational forecasts and analyses by the PREV'AIR system, J. Geophys. Res., 113, D04301, doi:10.1029/2007JD008761, 2008.

Höpfner, M., Stiller, G. P., Kuntz, M., von Clarmann, T., Echle, G., Funke, B., Glatthor, N., Hase, F., Kemnitzer, H., and Zorn, S.: The Karlsruhe optimized and precise radiative transfer algorithm. Part II: Interface to retrieval applications, in: Optical Remote Sensing of the Atmosphere and Clouds, Beijing, China, 15–17 September 1998, edited by Wang, J., Wu, B., Ogawa, T., and Guan, Z., vol. 3501, pp. 186–195, 1998.

Kar, J., Fishman, J., Creilson, J. K., Richter, A., Ziemke, J., , and Chandra, S.: Are there urban signatures in the tropospheric ozone column products derived from satellite measurements?, Atmos. Chem. Phys., 10,

5213–5222, 2010.

Kar, J., Jones, D. B. A., Drummond, J. R., Attie, J.-L., Liu, J., Zou, J., Nichitiu, F., Seymour, M. D., Edwards, D. P., Deeter, M. N., Gille, J. C., and Richter, A.: Measurement of low-altitude CO over the Indian subcontinent by MOPITT, J. Geophys. Res., 113, D16307, doi:10.1029/2007JD009362, 2008.

Kobayashi, H., Shimota, A., Kondo, K., Okumura, E., Kameda, Y., Shimoda, H., and Ogawa, T.: Development and evaluation of the interferometric monitor for greenhouse gases: a high-throughput Fourier-transform infrared radiometer for nadir Earth observation, Appl. Opt., 38, 6801–6807, 1999.

Kopacz, M., Jacob, D. J., Fisher, J. A., Zhang, Z. L., Megretskaia, I. A., Yantosca, R. M., Singh, K., Henze, D. K., Burrows, J. P., Buchwitz, M., Khlystova, I., McMillan, W. W., Gille, J. G., Edwards, D. P., Eldering, A., Thouret, V., and Nedelec, P.: Global estimates of CO sources with high resolution by adjoint inversion of multiple satellite datasets (MOPITT, AIRS, SCIAMACHY, TES), Atmos. Chem. Phys., 10, 855–876, 2010.

Landgraf, J. and Hasekamp, O. P.: Retrieval of tropospheric ozone: The synergistic use of thermal infrared emission and ultraviolet reflectivity measurements from space, J. Geophys. Res., 112, D08310, doi:10.1029/2006JD008097, 2007.

Lee, S., Hong, Y., Song, C.-K., Lee, J., Choi, W.-J., Kim, D., Moon, K.-J., and Kim, J.: Plan of Korean Geostationary Environment Satellite over Asia-Pacific region, in: Geophysical Research Abstracts, Vol. 12, EGU2010-7595-1, EGU General Assembly, 2010.

Levelt, P. F., van den Oord, G. H. J., Dobber, M. R., Mslkki, A., Visser, H., Vries, J., Stammes, P., Lundell, J. O. V., and Saari, H.: The Ozone monitoring instrument, IEEE Trans. Geosci. Remote Sens., 44, 5, 1093–1101, doi:0.1109/TGRS.2006.872333, 2006.

Martin, R. V.: Satellite remote sensing of surface air quality, Atmos.-Environ., 42, 7823–7843, 2008.

Menut, L. and Bessagnet, B.: Atmospheric composition forecasting in Europe, Atmos.-Environ., 28, 61–74, 2010.

McMillan, W. W., Barnet, C., Strow, L., Chahine, M., McCourt, M., Novelli, P., Korontzi, S., Maddy, E., and Datta, S.: Daily global maps of carbon monoxide: First views from NASA's Atmospheric Infrared Sounder, Geophys. Res. Lett., 32, L11801, doi:10.1029/2004GL012,821, 2005.

National Research Council: Earth Science and Applications from Space: National Imperatives for the Next Decade and Beyond, in: the National Academy of Sciences, Washington, D. C, USA, 2007.

Orphal, J., Bergametti, G., Beghin, B., Hébert, J.-P., Steck, T., and Flaud, J.-M.: Monitoring tropospheric pollution using infrared spectroscopy from geostationary orbit, Comptes Rendus Physique, 6, 888–896, 2005.

Peuch, V.-H., Amodei, M., Barthet, T., Cathala, M.-L., Michou, M., and Simon, P.: MOCAGE, MOdéle de Chimie Atmosphérique à Grande Echelle, in: Proceedings of Météo France: Workshop on atmospheric modelling, pp. 33–36, Toulouse, France, 1999.

Peuch, V.-H., Attié, J.-L., Claeyman, M., Amraoui, L. E., Ricaud, P., Semane, N., Massart, S., Piacentini, A., Cariolle, D., Flaud, J.-M., Bergametti, G., Cantie, R., Pasternak, F., Lehors, L., von Clarmann, T., Höpfner, M., and Orphal, J.: Data assimilation experiments within the POGEQA project, in: American Geophysical Union, Fall Meeting, San Francisco, California, USA, December, 2009.

Peuch, V.-H., Orphal, J., and the MAGEAQ consortium: MAGEAQ: Monitoring the Atmosphere from Geostationary orbit for European Air Quality, Proposal submitted to ESA for Earth Explorer Opportunity Mission EE–8, 2010.

Pfister, G., Pétron, G., Emmons, L. K., Gille, J. C., Edwards, D. P., Lamarque, J.-F., Attié, J.-L., Granier, C., and Novelli, P. C.: Evaluation of CO simulations and the analysis of the CO budget for Europe, J. Geophys. Res., 109, D19304, doi:10.1029/2004JD004691, 2004.

Phillips, D.: A technique for the numerical solution of certain integral equations of first kind, J. Ass. Comput. Mat., 9, 34–97, 1962.

Pierangelo, C., Hébert, P., Rosak, A., Buil, C., and Bernard, F.: SIFTI, a Static infrared Fourier Transform Interferometer dedicated to ozone and CO pollution monitoring, in: International TOVS Study Conference (ITSC XVI), 5-13 may 2008, Angra dos Reis, Brasil, 2008.

Pougatchev, N., August, T., Calbet, X., Hultberg, T., Oduleye, O., Schlussel, P., Stiller, B., Germain, K. S., and Bingham, G.: IASI temperature and water vapor retrievals, error assessment and validation, Atmos. Chem. Phys., 9, 6453–6458, 2009.

Rodgers, C. D.: Inverse Methods for Atmospheric Sounding: Theory and Practice, Series on Atmospheric, Oceanic and Planetary Physics, vol. 2, World Scientific, 2000.

Rothman, L. S., Jacquemart, D., Barbe, A., Benner, D. C., Birk, M., Brown, L. R., Carleer, M. R., Chackerian, J. C., Chance, K., Coudert, L. H., Dana, V., Devi, V. M., Flaud, J.-M., Gamache, R. R., Goldman, A., Hartmann, J.-M., Jucks, K. W., Maki, A. G., Mandin, J.-Y., Massie, S. T., Orphal, J., Rinsland, A. P. C. P., Smith, M. A. H., Tennyson, J., Tolchenov, R. N., Toth, R. A., Auwera, J. V., Varanasi, P., and Wagner, G.: The HITRAN 2004 molecular spectroscopic database, J. Quant. Spectrosc. Ra., 96, 139–204, 2005.

Rouïl, L., Honoré, C., Vautard, R., Beekmann, M., Bessagnet, B., Malherbe, L., Meleux, F., Dufour, A., Elichegaray, C., Flaud, J.-M., Menut, L., Martin, D., Peuch, A., Peuch, V.-H., and Poisson, N.: An Operational Forecasting and Mapping System for Air Quality in Europe, Bull. Amer. Meteor. Soc., 90, 1, 73–83, 2008.

Seinfeld, J. H. and Pandis, S. N.: Atmospheric Chemistry and Physics, from Air Pollution to Climate Change, John Wiley & Sons, 1997.

Shim, C., Li, Q., Luo, M., Kulawik, S., Worden, H., Worden, J., Eldering, A., Diskin, G., Sachse, G., Weinheimer, A., Knapp, D., Montzca, D., and Campos, T.: Satellite observations of Mexico City pollution outflow from the Tropospheric Emissions Spectrometer (TES), Atmos.-Environ., 43, 1540–1547, 2009.

Stiller, G. P., von Clarmann, T., Funke, B., Glatthor, N., Hase, F., Höpfner, M., and Linden, A.: Sensitivity of trace gas abundances retrievals from infrared limb emission spectra to simplifying approximations in radiative transfer modelling, J. Quant. Radiat. Transfer, 72 (3), 249–280, 2002.

Stuhlmann, R., Rodriguez, A., Tjemkes, S., Grandell, J., Arriaga, A., Bézy, J.-L., Aminou, D., and Bensi, P.: Plans for EUMETSAT's Third Generation Meteosat (MTG) Geostationary Satellite Program., Adv. Space Res., 36, 975–981, 2005.

Tikhonov, A.: On the solution of incorrectly stated problems and a method of regularization, Dokl. Acad. Nauk SSSR, 151, 501–504, 1963.

Turquety, S., Hadji-Lazaro, J., Clerbaux, C., Hauglustaine, D. A., Clough, S. A., Cassé, V., Schlüssel, P., and Mégie, G.: Operational trace gas retrieval algorithm for the Infrared Atmospheric Sounding Interferometer, J. Geophys. Res., 109, D21301, doi:10.1029/2004JD004821, 2004.

Turquety, S., Hurtmans, D., Hadji-Lazaro, J., Coheur, P.-F., Clerbaux, C., Josset, D., and Tsamalis, C.: Tracking the emission and transport of pollution from wildfires using the IASI CO retrievals: analysis of the summer

2007 Greek fires, Atmos. Chem. Phys., 9, 4897–4913, 2009.

Vautard, R., Builtjes, P., Thunis, P., Cuvelier, K., Bedogni, M., Bessagnet, B., Honoré, C., Moussiopoulos, N., Schaap, M., Stern, R., Tarrason, L., and M. van Loon, M.: Evaluation and intercomparison of Ozone and PM10 simulations by several chemistry-transport models over 4 European cities within the City-Delta project, Atmos.-Environ., 41, 173–188, 2007.

Worden, J., Liu, X., Bowman, K., Chance, K., Beer, R., Eldering, A., Gunson, M., and Worden, H.: Improved tropospheric ozone profile retrievals using OMI and TES radiances, Geophys. Res. Lett., 34, L01809, doi: 10.1029/2006GL027806, 2007.

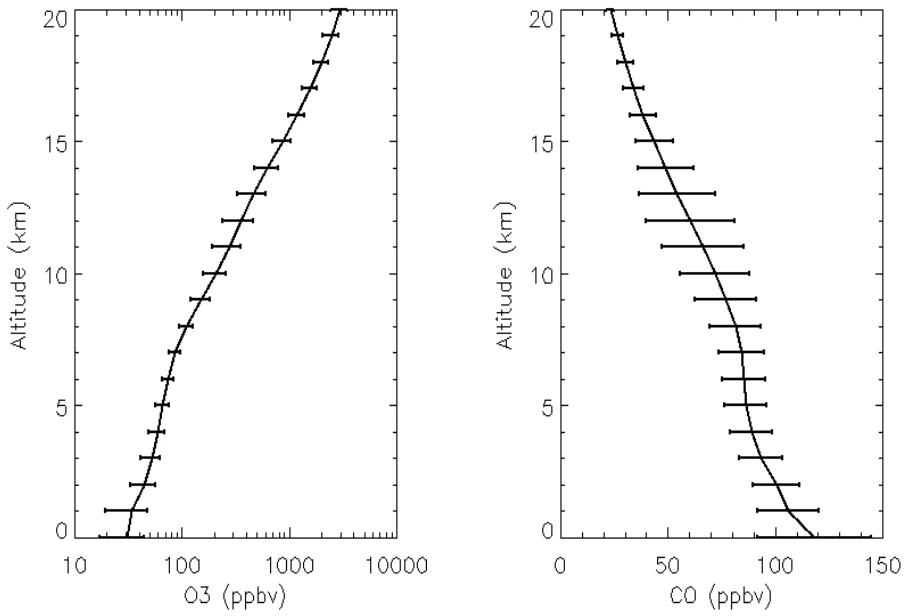

Fig. 1. MOCAGE O_3 and CO a priori profiles and variances (diagonal elements of $\boldsymbol{S}_e$ considered in this study.

Table 1. GEO-TIR and GEO-TIR2 instrument characteristics in the O_3 and CO thermal infrared band: Spectral Sampling Interval (SSI), Noise Equivalent Spectral Radiance (NESR) and Signal to Noise Ratio (SNR) calculated for a surface temperature of 280 K.

Sensor	Band	SSI (cm^{-1})	NESR ($nW/(cm^2.sr.cm^{-1})$)	SNR
GEO-TIR	O_3	0.05	6.04	750
GEO-TIR	CO	0.05	1.00	190
GEO-TIR2	O_3	0.625	24.5	180
GEO-TIR2	CO	0.625	6.12	30

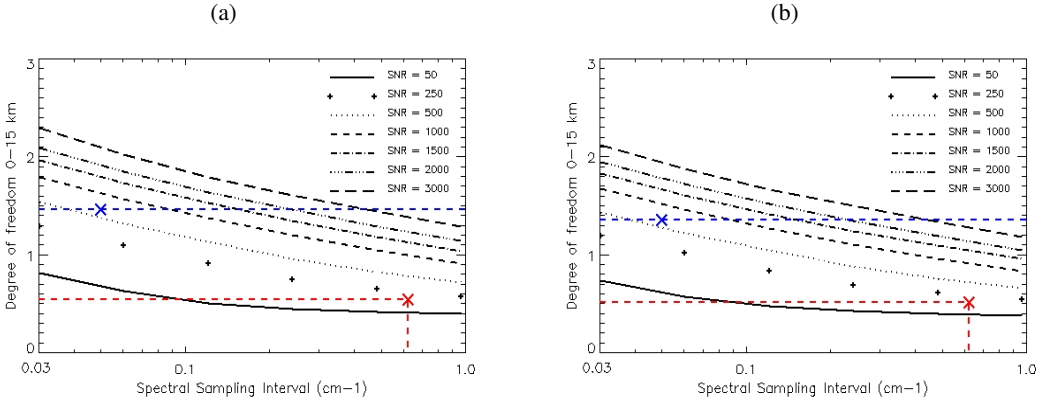

Fig. 2. Degrees of freedom (DOF) obtained for the O_3 retrieval as a function of spectral sampling interval and instrument noise (SNR): (a) positive thermal constrast (+2 K); (b) negative thermal contrast (-2 K). The DOFs have been obtained for an idealized case where all the parameters (e.g, regularization) are fixed except the SNR and the spectral resolution. The reference profile used to generate the synthetic measurement spectral radiances and representing the true profile in the retrieval study is an average of MOCAGE O_3 over Europe from July 1^{st}, 2009 to August 31^{th}, 2009 during daytime for the positive thermal contrast and during nighttime for the negative thermal contrast. The SNR is calculated for a surface temperature of 280 K. The blue cross corresponds to the GEO-TIR instrument configuration and the red cross corresponds to GEO-TIR2 instrument configuration.

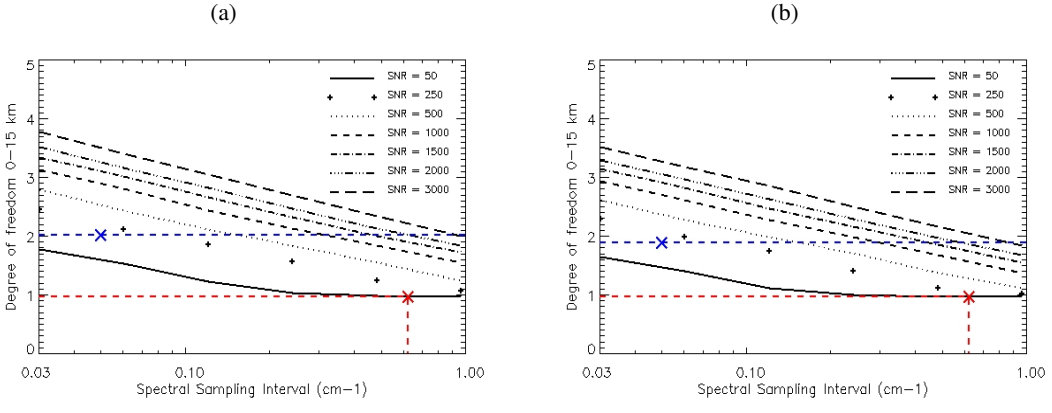

Fig. 3. Same as Figure 2 but for CO.

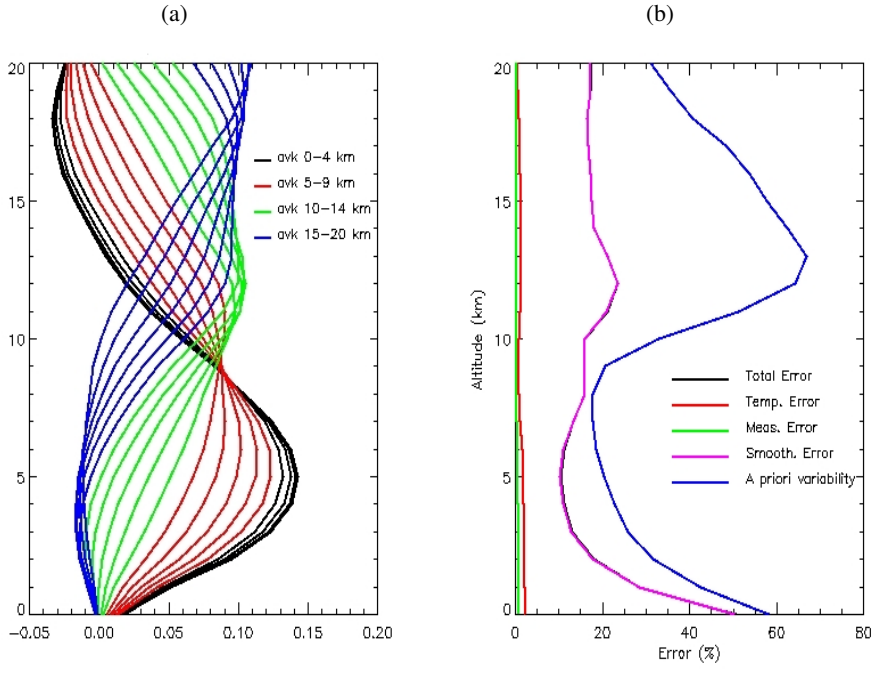

Fig. 4. (a) Averaging kernels obtained for the O_3 retrieval for a thermal contrast of 0 K: spectral sampling interval of 0.05 and a Signal to Noise Ratio (SNR) of 750 (0-4 km: black, 5-9 km: red, 10-14 km: green, 15-20 km blue); (b) error budget as a function of altitude for different error sources (see legend) for the same instrument characteristics as in part (a).

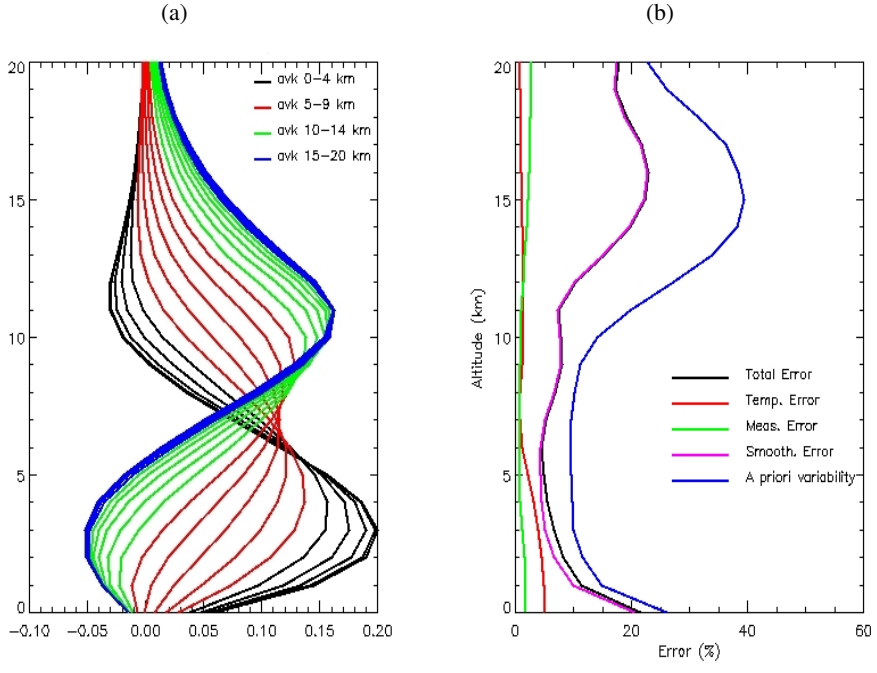

Fig. 5. Same as Figure 4 but for CO.

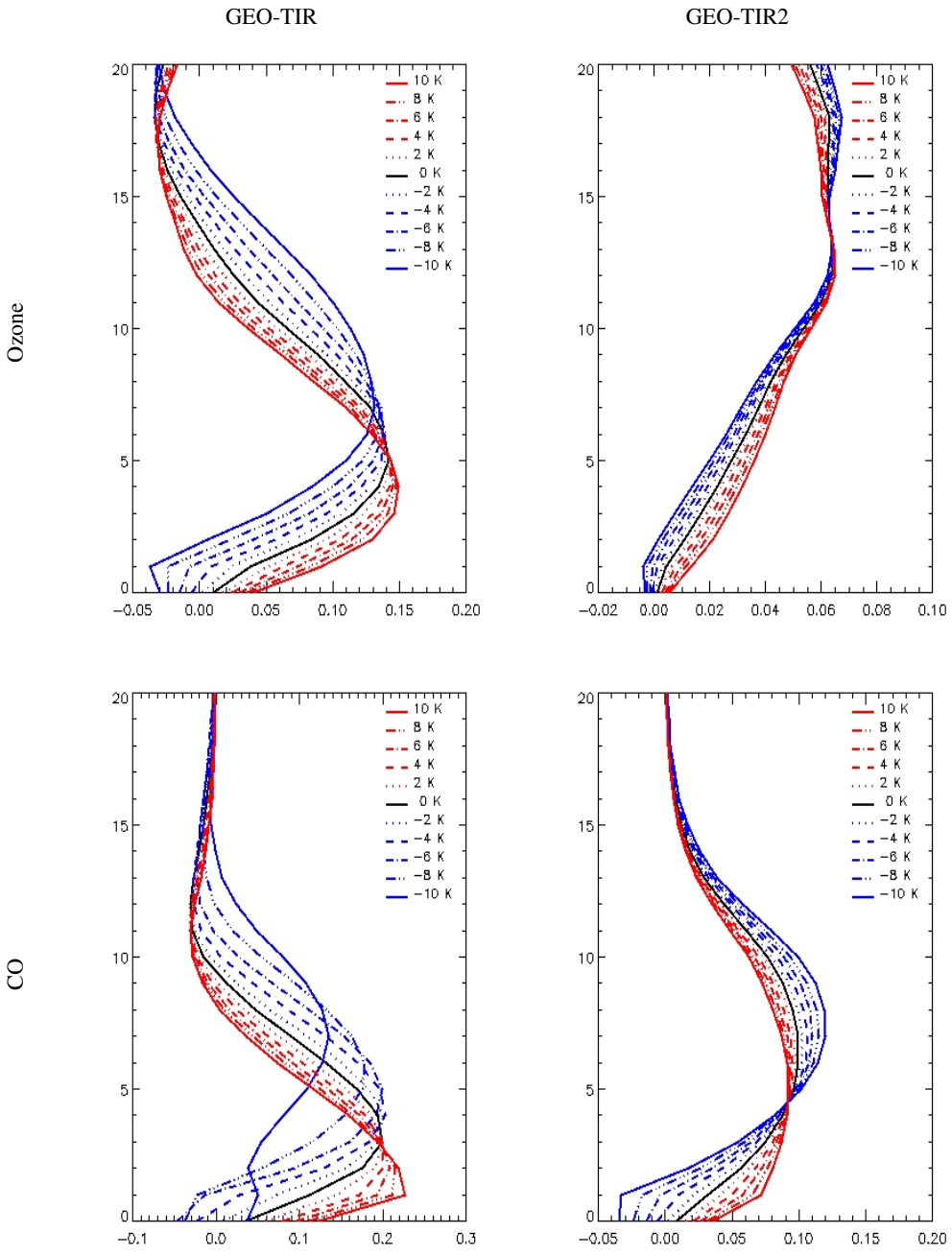

Fig. 6. First averaging kernel (surface level) calculated for different thermal contrasts from -10 K to 10 K for GEO-TIR (left) and GEO-TIR2 (right) for O_3 (top) and CO (bottom). Blue averaging kernels correspond to negative thermal contrast, red averaging kernels correspond to positive thermal contrast and the black averaging kernel correspond to a thermal contrast equal to 0 (see legend for line style).

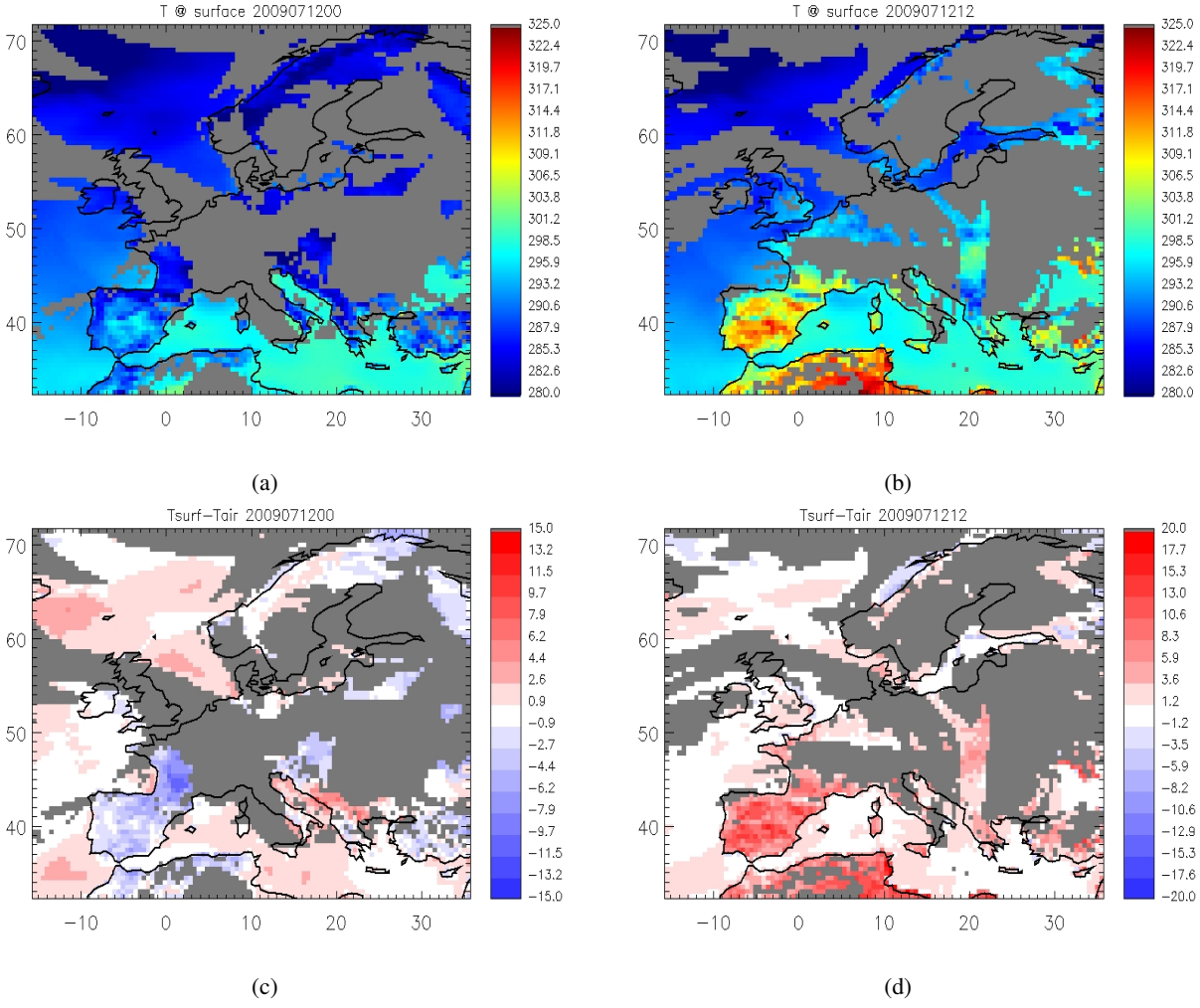

Fig. 7. Surface temperature in K (a,b) and thermal contrast (surface temperature minus air temperature near the surface) in K (c,d) on July 12^{th}, 2009 from ARPEGE: (left) 00 UTC; (right) 12 UTC. Grey areas represent pixels with more than 50% of cloud fraction. In (c,d) red indicates surface temperature is higher than the air temperature; blue indicates surface temperature is lower than the air temperature.

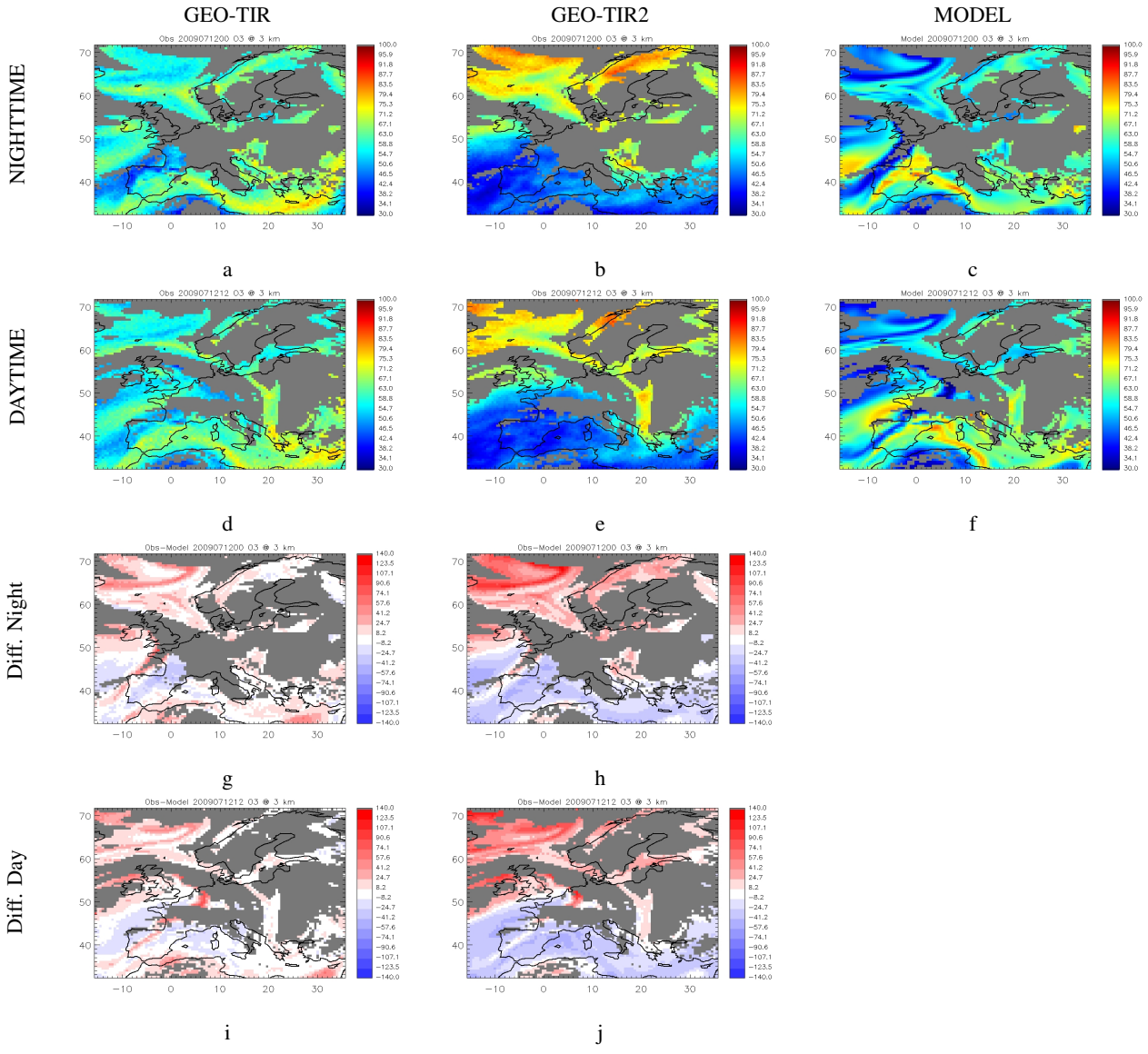

Fig. 8. O_3 fields in parts per billion by volume (ppbv) at 3 km on July 12^{th}, 2009 at 00 h UTC (nighttime: top and third row) and at 12 h UTC (daytime: second and bottom row) simulated by the MOCAGE model (c and f), and simulated by the Geostationary Oberving System of GEO-TIR (a and d) and GEO-TIR2 (b and e) instruments. Relative difference (%) between simulated observations and model are shown for GEO-TIR (g and i) and for GEO-TIR2 (h and j) for nighttime (g and h) and daytime (i and j). Grey areas represent pixels with more than 50% of cloud fraction. In panels g-j, red indicates simulated observations are higher than the model results; blue indicates simulated observations are lower than the model results.

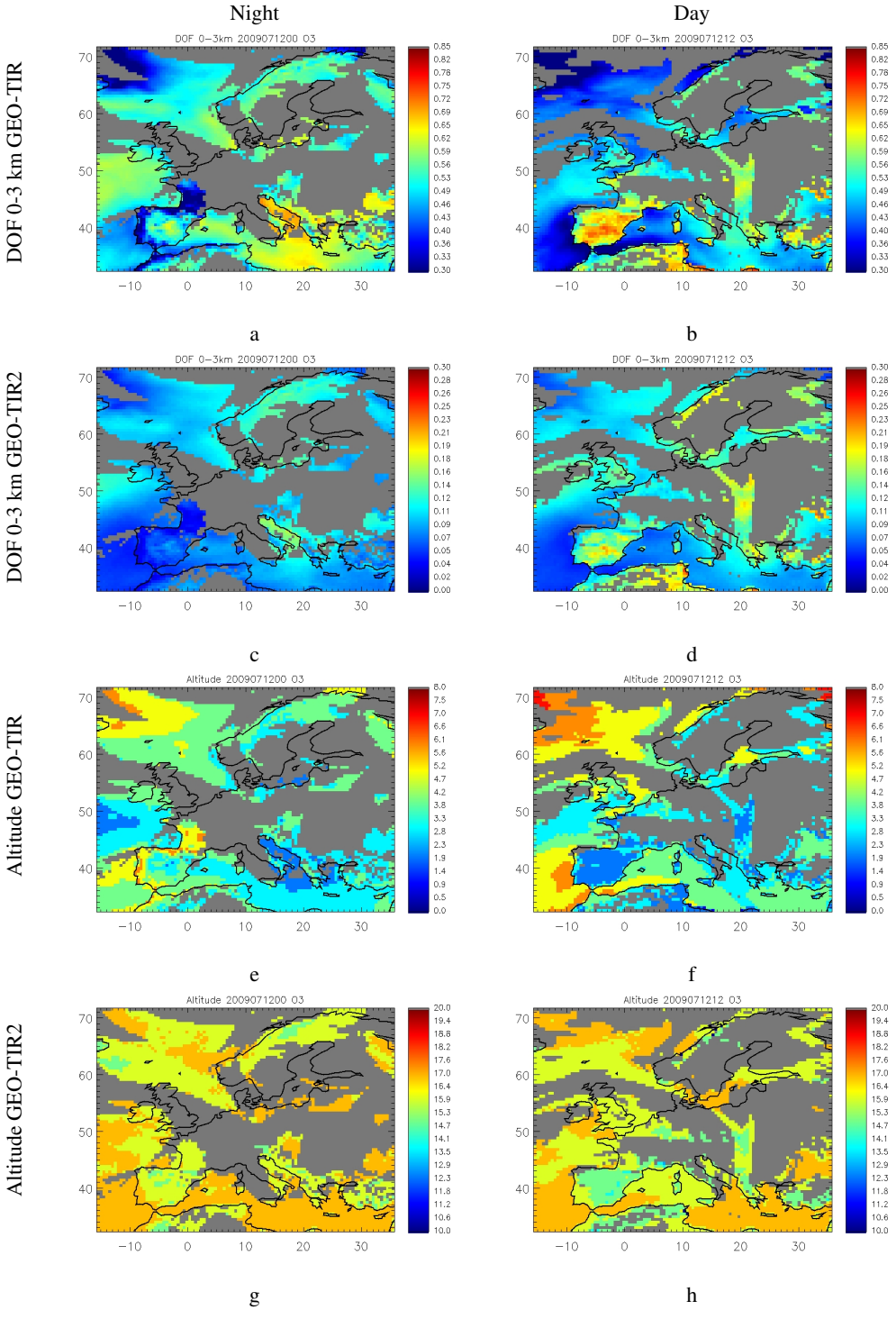

Fig. 9. Degrees of Freedom obtained for O_3 with GEO-TIR (a,b) and with GEO-TIR2 (c,d) instrument configuration on July 12^{th}, 2009 at 00 h UTC (left) and at 12 h UTC (right). The peak altitude (km) of the lowermost averaging kernels are represented for GEO-TIR (e,f) and for GEO-TIR2 (g,h) on July 12^{th}, 2009 at 00 h UTC (left) and at 12 h UTC (right) . Grey areas represent pixels with more than 50% of cloud fraction. Note that the colour scales are different for GEO-TIR and GEO-TIR2.

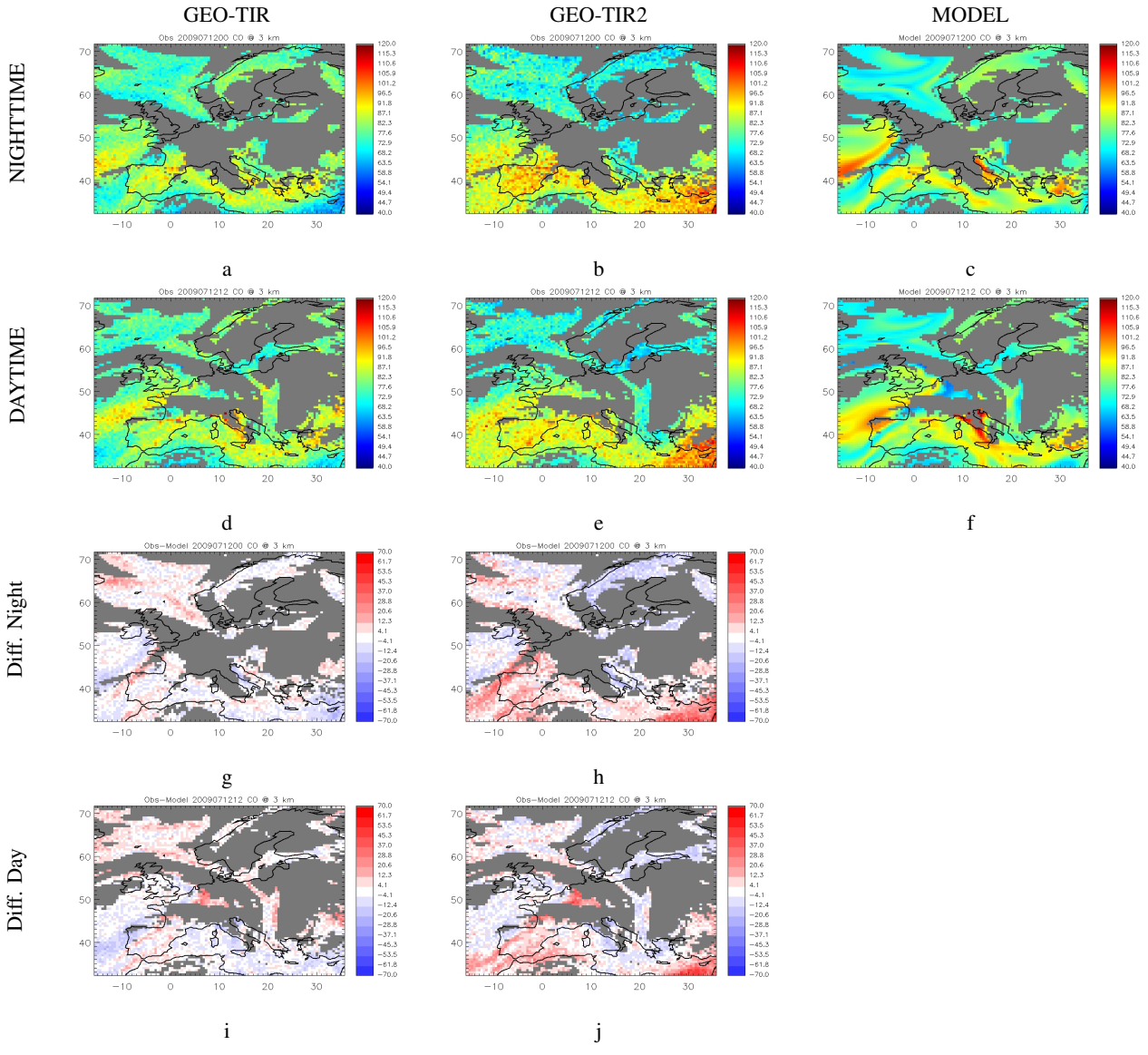

Fig. 10. Same as Figure 8 but for CO.

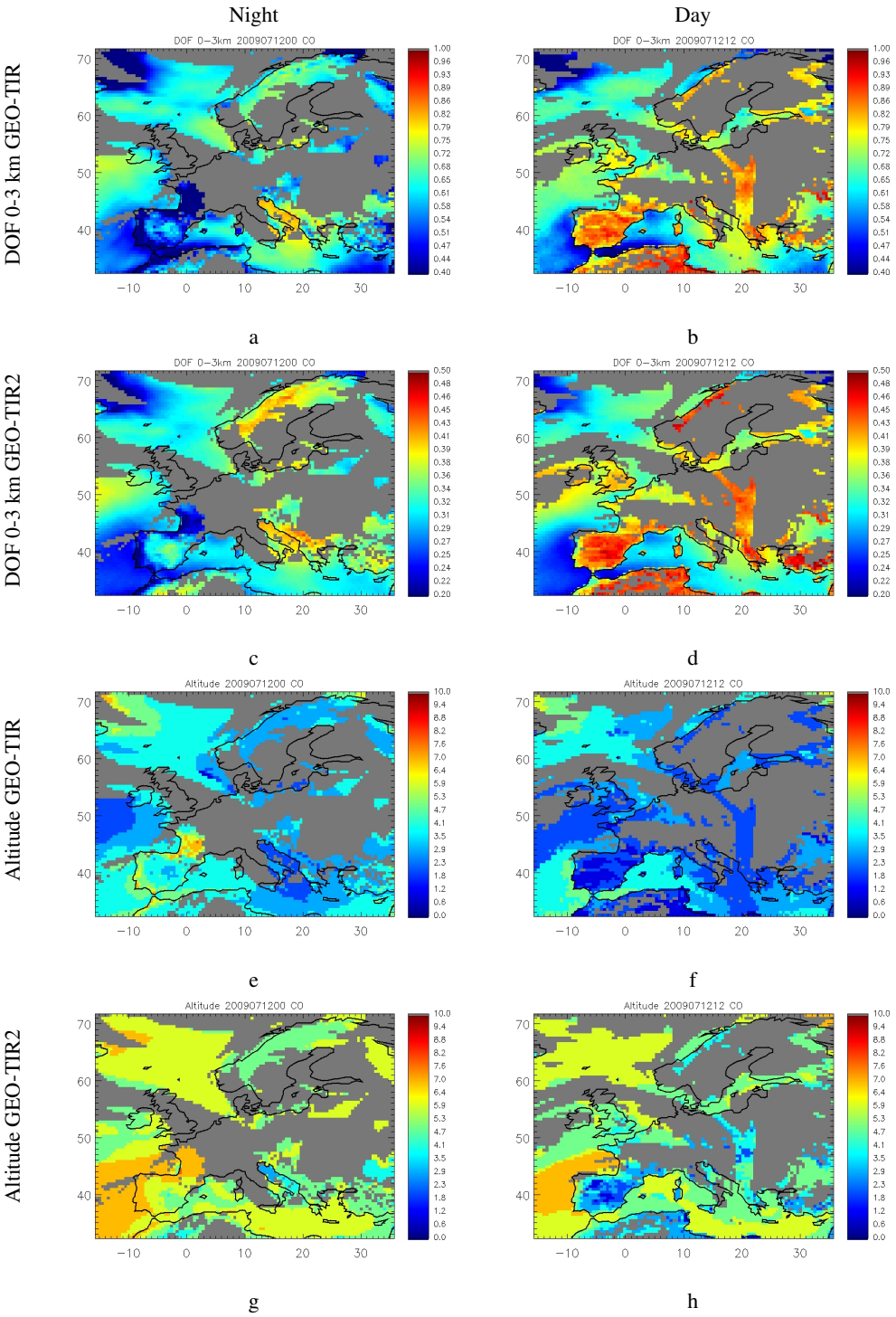

Fig. 11. Same as Figure 9 but for CO.

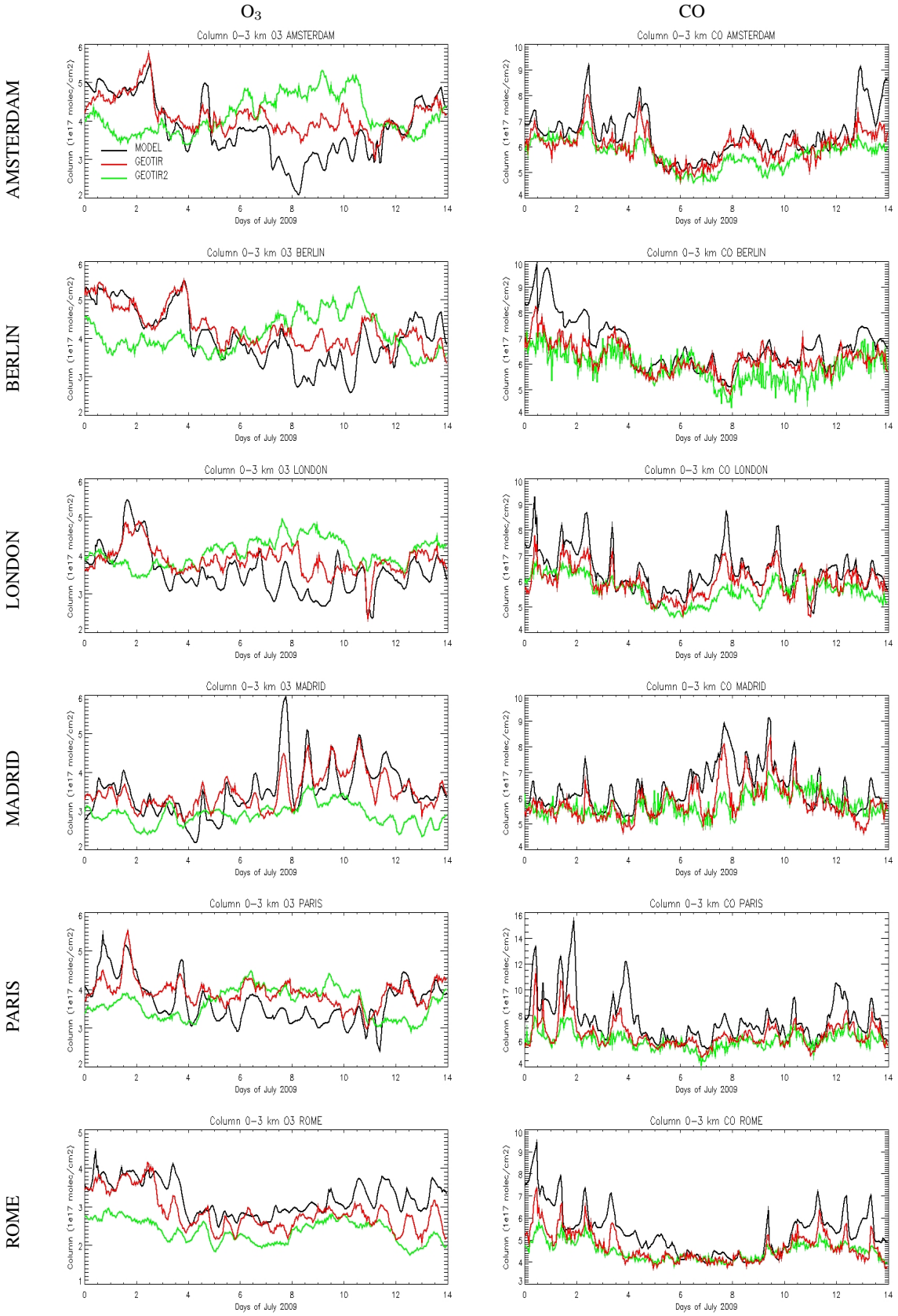

Fig. 12. Time-series of O_3 (left) and CO (right) 0-3 km column (molecules/cm^2) from July, 1^{st} 2009 to July, 15^{th} 2009 with a temporal resolution of 1 hour from the model MOCAGE (black line), GEO-TIR (red line) and GEO-TIR2 (green line) over 6 European cities, top to bottom panels: Amsterdam, Berlin, London, Madrid, Paris and Rome.

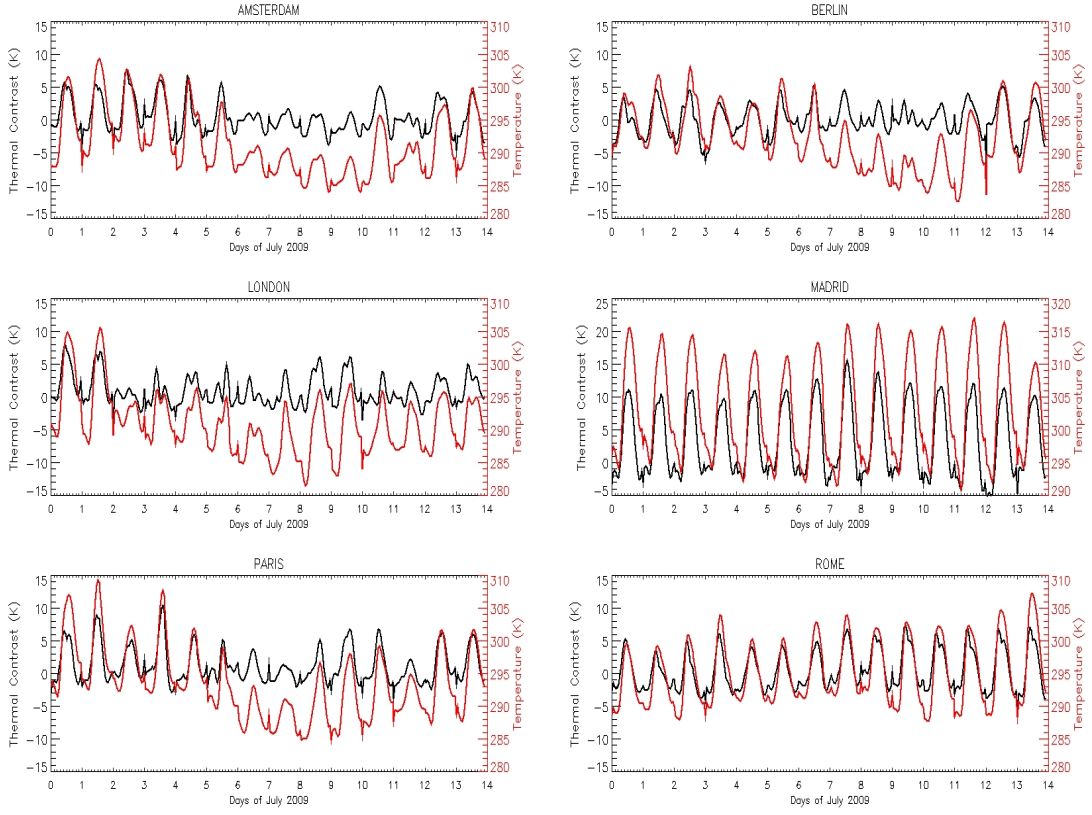

Fig. 13. Time-series of temperature at surface (red) and thermal contrast (black) in K from ARPEGE model from July, 1^{st} 2009 to July, 15^{th} 2009 with a temporal resolution of 1 hour over 6 European cities: Amsterdam, Berlin, London, Madrid, Paris and Rome.

Table 2. Correlation (corr) bias and standard deviation (stdev) of the O_3 0-3 km and 0-6 km columns (molecules/cm^2) between MOCAGE model and GEO-TIR observations and between MOCAGE model and GEO-TIR2 observations for 6 European cities: Amsterdam, Berlin, London, Madrid, Paris and Rome. Positive bias indicate that observations are higher than MOCAGE and negative bias indicate than observations are lower than MOCAGE.

CITY	Column 0-3 km						Column 0-6 km					
	GEO-TIR - MOCAGE			GEO-TIR2 - MOCAGE			GEO-TIR - MOCAGE			GEO-TIR2 - MOCAGE		
	Corr	**Bias %**	**Stdev %**	**Corr**	**Bias %**	**Stdev %**	**Corr**	**Bias %**	**Stdev %**	**Corr**	**Bias %**	**Stdev %**
AMST.	0.81	10.3	16.8	-0.57	14.3	35.1	0.82	7.5	11.1	-0.54	10.0	27.3
BERLIN	0.81	6.5	12.7	-0.46	5.3	28.7	0.82	4.5	10.5	-0.42	2.9	25.0
LONDON	0.73	10.5	12.2	-0.37	17.8	22.8	0.78	8.6	8.7	-0.33	14.5	18.8
MADRID	0.73	0.8	12.9	0.30	-15.3	15.0	0.86	-1.5	6.9	0.47	-16.0	10.3
PARIS	0.71	7.8	11.3	-0.16	1.3	19.0	0.74	4.8	8.1	-0.14	-1.7	15.7
ROME	0.76	-11.4	9.4	0.52	-25.9	9.2	0.92	-7.9	6.2	0.66	-21.5	8.3

Table 3. Same as Table 2 but for CO.

CITY	Column 0-3 km						Column 0-6 km					
	GEO-TIR - MOCAGE			GEO-TIR2 - MOCAGE			GEO-TIR - MOCAGE			GEO-TIR2 - MOCAGE		
	Corr	**Bias %**	**Stdev %**	**Corr**	**Bias %**	**Stdev %**	**Corr**	**Bias %**	**Stdev %**	**Corr**	**Bias %**	**Stdev %**
AMST.	0.83	-5.9	6.6	0.71	-10.6	7.9	0.89	-4.1	4.7	0.78	-8.1	6.1
BERLIN	0.83	-6.6	7.2	0.68	-11.5	9.0	0.89	-4.5	5.2	0.73	-8.7	7.5
LONDON	0.84	-6.1	6.2	0.64	-10.8	8.5	0.91	-4.1	3.9	0.76	-8.0	6.1
MADRID	0.79	-7.3	6.9	0.39	-8.4	10.5	0.86	-4.9	4.7	0.52	-5.0	8.1
PARIS	0.81	-13.9	9.7	0.66	-19.1	12.1	0.85	-9.6	7.3	0.72	-13.9	9.6
ROME	0.82	-11.6	9.7	0.74	-14.2	11.5	0.90	-6.0	6.0	0.85	-7.9	7.3